


SURVEY PAPER

Advances in unsteady computational aerodynamics with separation: The 61st Lanchester memorial lecture

M. J. Smith 

Daniel Guggenheim School of Aerospace Engineering, Georgia Institute of Technology, Atlanta, GA, USA
Email: ms55@gatech.edu

Received: 2 April 2025; **Revised:** 26 May 2025; **Accepted:** 28 May 2025

Keywords: aerodynamics; CFD; dynamic stall; flow separation; gusts; rotorcraft; transition; turbulence

Abstract

This paper is based on the Lanchester Lecture of the Royal Aeronautical Society held in London, UK, in October 2023. The lecture discussed the advances in computational modeling of separated flows in aerospace applications since Elsenaar's Lanchester Lecture in 2000. Elsenaar's efforts focused on assumptions primarily associated with separation for steady inflow and a static (non-moving) vehicle or component. Since that time, significant advancements in computational hardware, coupled with substantial investments in the development of algorithms and solvers, have led to important breakthroughs in the field. In particular, computational aerodynamics techniques are currently applied to complex aerospace problems that include unsteady or dynamic considerations, such as dynamic stall and gusts, which are discussed. A perspective of the technology developed over the past quarter-century, highlighting their importance to computational aerodynamics is discussed. Finally, the potential of future areas of development, such as machine learning, that may be exploited for the next generation of computational aerodynamics applications is explored.

Nomenclature

b	wing or aerofoil semi-chord, $b = \frac{c}{2}$
c	wing or aerofoil chord
C_D	drag coefficient
C_p	pressure coefficient
k	turbulent kinetic energy
k_f	reduced frequency, $k = \frac{\omega_f b}{V}$
M_∞	freestream Mach number
N_y	number of points in span direction
Re	Reynolds number
t	time
T	period of oscillation
x, y, z or X, Y, Z	chord, span and normal axes, respectively
x_{tr}	chord location of transition

Greek symbol

α	angle-of-attack
Φ	nondimensional period of oscillation, $\frac{t}{T}$
ψ	angle defining rotor revolution oriented from aft rotor disk point parallel to wind, assumed to be counterclockwise
θ	angle of orientation measured from forward stagnation point

This paper is based on the 2023 Lanchester Lecture held in London at the Royal Aeronautical Society.

ω	rate of dissipation of the turbulence kinetic energy into internal thermal energy
ω_f	frequency of oscillation

1.0 Introduction

The Lanchester Memorial lecture honors Frederick William Lanchester (1868–1946), one of Great Britain's pioneers in aviation. Dr. Lanchester's seminal contributions encompassed the fields of mechanical engineering, aeronautical engineering and operations research, as well as music, poetry and mathematics [1–4].

1.1 Lanchester's contributions

While Dr. Lanchester contributed to many disciplines within aeronautical engineering, arguably his most important advancements lie within aerodynamics. He published two seminal aerodynamic concepts in his 1907 text *Aerodynamics* [5], the first of a two-part series entitled *Aerial Flight*. These concepts were a fundamental step in understanding the physics of translating and rotating air vehicle lifting surfaces.

There are three primary concepts from Lanchester's body of research that directly relate to the topic of this publication. First published in *Aerodynamics*, but introduced earlier in 1894, Lanchester proposed his 'vortex theory of lift' wherein lift is sustained through circulation on finite wings. He established many concepts ubiquitous in lifting-line and wake models applied today, including circulation, bound and trailing vorticity, induced drag and aspect ratio. One of his many sketches on the topic, published in a later paper in 1915 [6] and included as Figure 1, illustrates his theoretical development on finite wing circulation. His work influenced Prandtl's development of lifting line theory [7], and it is recognised by many as the Lanchester-Prandtl lifting line theory [8]. Lanchester discerned that his theory was applicable also to rotating wings (propellers, rotors), and he posited the helical character of and vortex interactions in rotor wakes in *Aerodynamics* and his later works [9].

The second concept introduced by Lanchester is the influence of viscous drag on separation. Samuel Langley's proposition in 1891 that skin friction played a negligible role in drag [8, 10] was accepted for about 15 years. Lanchester's experiments from 1905 to 1907 proved the converse of Langley's assumption, that skin friction was a prime constituent in what is now defined as viscous drag in aerofoils and wings [5, 11]. Further, he demonstrated an understanding of smooth separation, identifying the concepts of separation bubbles, trailing edge separation and stall. With regard to flow separation on smooth surfaces, skin friction influences boundary layer behaviour which in turn leads to flow separation. He delved into the concept of stall, recognising that the aerodynamic characteristics of the wing changed with higher angles of attack when the flow no longer remained attached, per his sketches such as Figure 2 [5].

Finally, as exemplified in prior Lanchester lectures by Collar [12], Jones [13] and Rogers [14], Lanchester is regarded as a pioneer in the development of the field of unsteady aerodynamics. Lanchester was consulted on early issues with aircraft flutter which was a problem in the 1910s and 1920s. He recognised that the variation of aerodynamics played a key role in aeroelasticity and encouraged the United Kingdom (UK) National Physical Laboratory to experimentally study the concept, leading to the field of unsteady aerodynamics.

Lanchester's early role in identifying these fundamentals of flow characteristics is foundational when developing computational methodologies to predict the flow separation for air vehicles, in particular when they undergo dynamic motion including control and lifting surface oscillations and rotations or vehicle maneuvers.

1.2 Characteristics of flow separation

In the 2000 Lanchester Memorial lecture, Elsenaar examined the topic of aerodynamic flow separation, with and without the presence of vortices [15]. Elsenaar emphasised the then current knowledge of the

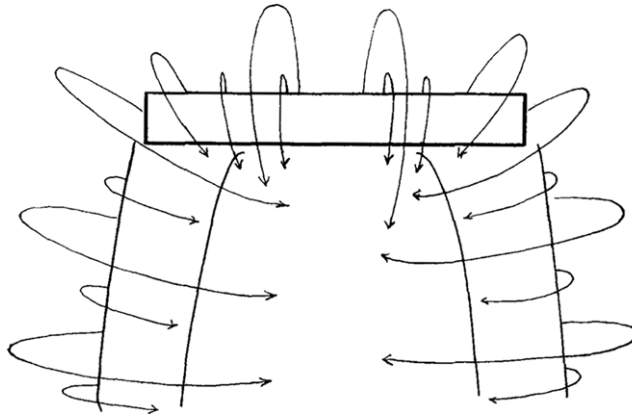


Figure 1. Lanchester's vortex theory of lift included the concept of bound and trailing vortices (Figure 6 from Ref. [6]).

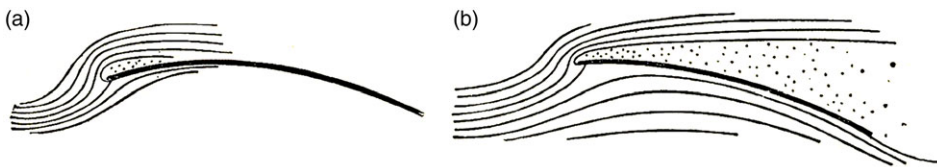


Figure 2. Lanchester's illustrations of smoothly separated flow for a separation bubble near the leading edge (left) and a fully separated aerofoil (right). Figure from Ref. [5].

physics of flow separation and predictive capabilities for fixed-wing applications, including analytical models, to develop a topological map of the types of flow separation. Many of the separation criteria from Elsenaar's earlier work are still applicable or extensible to unsteady flow separation.

Whether the vehicle is static or dynamically moving within a freestream velocity field, three-dimensional boundary layer flow separation can be categorised as local or global. Local separation occurs when, as Elsenaar described, 'bubble-like' behaviour is observed where in the flow cannot overcome an adverse pressure gradient. Examples can include laminar separation bubbles and separation that occurs near the trailing edge of aerofoils and wings. These can also occur when the flow or the geometry introduces a discontinuity, such as shock-induced separation bubbles or the separation behind bluff bodies.

The second form of separation occurs from the interaction with vortical flows, either in the form of a single vortex or a vortex sheet. Examples include vortices formed due to notched leading-edges of wings, finite tips or pointed forebodies. Discontinuities in the external structure, such as vehicle component junctions and gaps between lifting and control surfaces can also produce vortices that depart the surface and result in separation. Sharp leading edges at angles of attack develop vortex sheets that can produce massive separation over wings. The separation associated with vortices has a more global effect on the vehicle aerodynamic performance.

The introduction of vehicle dynamic motion or variations in Mach or Reynolds number can act to mitigate or exacerbate the separation behaviour over a surface. Small local smooth separations can grow and create vortex sheets leading to large separations. This can be the case with increases of the wing angle-of-attack beyond static stall with or without rotation. These unsteady vortex-surface aerodynamic interactions – including scenarios where shed vorticity impinges downstream surfaces (tails), as well as blade-vortex interactions in rotating systems – lead to aeroelastic phenomena, just as Lanchester hypothesised over a century ago.

1.3 Computational aerodynamics

The field of aerodynamics is erroneously characterised by some as a ‘mature’ field, not worthy of further research development in the 21st century. This is completely untrue as some of the most difficult aspects of vehicle flight are rooted in the realm of unsteady aerodynamics, and this is especially crucial to progress in the fields of aeroelasticity, flight controls and flow control.

Computational aerodynamics of separated flows is a broad field of discussion, so the focus in this work will be concentrated primarily on some specific developments and applications that have advanced in the last quarter century since the Elsenaar’s 2000 Lanchester lecture [15]. It is impossible to cite every contribution made by the worldwide community, so examples to illustrate various aspects of the issues are included but should not be considered as indicative of the only important contributions to the field.

2.0 Computational frameworks for complex dynamic motion

Aerodynamics and its broader counterpart fluid mechanics are by definition unsteady. Researchers have spent many years developing simplifications to provide steady solutions to static (inertial frame) engineering problems, but these have been limited for the most part by the computational capabilities available at the time of development. Many of the tools necessary to resolve the unsteadiness of aerodynamic applications arguably did not become a reality until the last decade of the 20th century.

While interest in the computational assessment of separation began with the advent of the computer itself, progress has been dictated by the limits of computer hardware. Since the concept was introduced in 1965, Moore’s law has been the popular measure of the rate of progress in computational capabilities [16]. It is based on the assumption that the number of transistors on a microchip doubles every two years, while the cost of computers is halved. While the current efficacy of Moore’s law is under discussion as the scaling moves away from hardware dimensionality [17], it provides accurate estimates of the historical development of computing capabilities. Computer hardware limitations have impacted both the spatial and temporal facets of unsteady computations: the lack of memory for the refined meshes necessary to capture flow separation, and the computer (and wall) clock time required to resolve the refined time-accurate integration of the fluid interaction.

An increase in computational memory hardware paralleled the development of faster processors. A shift in computer memory hardware occurred in the 1970s when semiconductor memory replaced core memory with the invention of dynamic random access memory (DRAM), which is still applied today in conventional central processing units (CPUs).¹ Current CPU memory systems are composed of a collection of dual inline memory modules (DIMMs) that contain multiple DRAM chips [18]. When the DRAM chip was patented in 1968 [19], it had a capacity of one kilobit (1 kb). Modern DRAM chips can store up to eight Gigabits (8 Gb) [18], so that modern HPC clusters may contain over a 1,000 computing nodes with 200 – 500 gigabytes (GB) memory per node [20]. These large parallel processing memory systems are required so that mesh sizes to capture moving and stationary frames over the time of interest are sufficiently refined to capture the boundary layer separation and near-wake physics.

Before the start of the new millennium, the solution of the Navier-Stokes equations for separated flow aerodynamics and aeroelastic simulations with dynamic motion was in its infancy, as illustrated in Figure 3. The introduction of high-performance parallel computing clusters in the late 1990s [21] (when the term ‘high performance computing’ also replaced ‘supercomputing’ in the technical verbiage) corresponded with the availability of sufficient computational memory so that significant inroads could be achieved into the development of algorithms and their application to unsteady aerodynamics problems of interest. Figure 3 highlights important breakthroughs in software development and applications in the fixed- and rotary-wing sectors (red and blue, respectively, with platform independent contributions in purple).

¹While graphical processing units (GPUs) are rapidly becoming pivotal to accelerate numerical solutions, this discussion will focus on CPU memory systems that still remain the standard for most unsteady Reynolds averaged Navier-Stokes (uRANS) applications today.

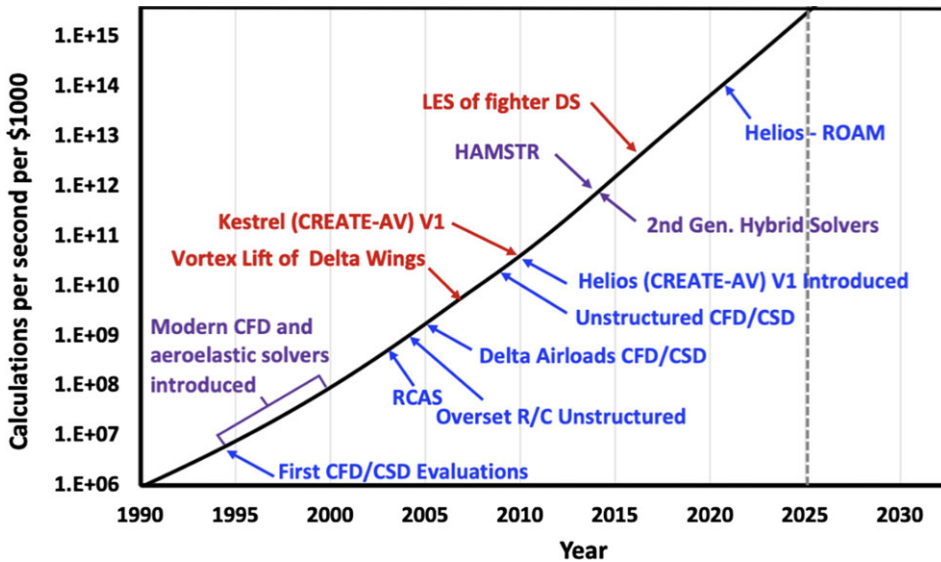


Figure 3. Development of computational capabilities for dynamic, separated flows as compared with Moore's Law. Blue = rotary-wing, red = fixed wing, Purple = both.

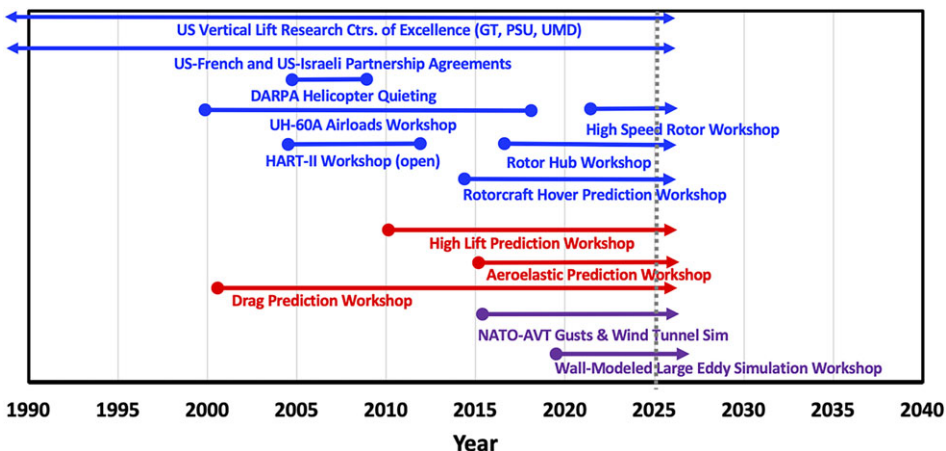


Figure 4. Successful collaborations that have focused on resolution of topics important to computational unsteady, separated flows. Blue = rotary-wing, red = fixed wing, Purple = both.

Significant achievements in this complex field were accelerated when successful collaborations were formed to address a specific topic of interest. This is contrary to Lanchester, who preferred to work independently. Using the same colour scheme as Figure 3, the collaborations depicted in Figure 4 have been responsible for some of the major breakthroughs thus far in the 21st century. Thus, collaborations should be encouraged to bring individuals with different expertise and solvers to understand and computationally resolve the intricacies of these complex physics.

Concurrent with computational hardware, the introduction of new computational methods – including aeroelastic computational methods, acoustics predictions, unstructured code usage, advanced turbulence modeling and the US DOD CREATE™-AV computational frameworks, such as Kestrel [22] and Helios [23, 24] – have all played a significant role during the past two decades of progress, as illustrated in Figure 3. In the US, the Defense Advanced Research Projects Agency (DARPA) Helicopter

Quieting Program [25, 26] sparked new interest in the development of advanced turbulence closures, such as large eddy simulation (LES)-based hybrid uRANS-LES wake models.

None of these advances would be possible without the computational frameworks to solve them. CREATETM-AV has arguably the most advanced computational framework available, but other open source tools such as SU2 from Stanford [27], commercial solvers and individual academic solvers have many capabilities as well. Complex geometries are modeled with structured or unstructured meshes, as best suits the component. Different solvers work together to reduce solution costs to provide efficient results. Coupling with structural dynamics tools, acoustics solvers and flight dynamics codes are also now relatively common.

No matter how sophisticated the computational tools, best practices are required to generate accurate solutions. Rogers, in the 21st Lanchester Memorial lecture in 1981, noted ‘The availability of computers does not absolve us from thinking deeply about the fluid-dynamic nature of the problem’ [14]. Indeed, the community needs to be even more cognisant and careful of the causal physics and flowfield phenomena that influence computational simulations. Physics influence the computational process from idea inception through mesh generation and simulation to post-processing and analysis.

2.1 Meshes

The engineer needs to ensure that the computational mesh is sufficient to capture the phenomena that drive and arise from the anticipated separation physics, as well as a timestep sufficient to capture the dynamic motion. The first and most important aspect of meshing is understanding that separation is a three-dimensional process. Two-dimensional Navier-Stokes simulations were performed by necessity in the 1980s due to computational limitations. It was apparent that, while a single plane would provide a general qualitative assessment, it could not accurately capture all of the salient details of separated flow, even without dynamic motion. Unfortunately, even today some users persist in attempting to predict static and dynamic separation with a single plane. They perhaps erroneously assume that physical aerofoil experiments describe an aerofoil undergoing separation in two dimensions, despite the fact that the experimental data were informed by a three-dimensional flow.

Computational fluid dynamic solvers, no matter their formulation, rely on refined meshes in the regions where the flow is rapidly changing, including areas where laminar-to-turbulent transition may occur. Mesh independence studies are routine practices in computational aerodynamics to ensure the mesh is sufficiently accurate to capture the physical phenomena of interest. Since these studies are computationally expensive, most focus on the streamwise – normal planes (e.g., planes at constant wing span or blade radius locations). Exemplar studies for aerofoil separated flows include Szydlowski and Costes [28] and Smith et al. [29]. Best practices, in addition to the well-known wall spacing ($y^+ \leq 1$), recommend that the mesh must include sufficient points orthogonal to the surface (20 – 60) to capture the onset of separation within the smooth surface boundary layer, and the normal cell size growth rate should be limited to 10% [28, 30, 31]. The span or radial surface mesh requirements are typically overlooked, but meshes that expand too quickly from the refined edge regions or large aspect ratios can cause problems in capturing separation. Kolpitcke and Smith [32] provide further best practices guidance for both translating and rotating lifting surface meshes. In their study, they quantified the role that radial mesh refinement, including chord-to-span mesh aspect ratio, has on the accurate prediction of these separated flows.

Meshes can be constructed of structured hexahedron elements assembled from two-dimensional quadrilateral sides. Unstructured meshes can be composed of multiple element shapes, and a tetrahedon is the most common element applied as it can easily conform to corners and other discontinuities in the geometry. Prisms, which replicate a length-diagonal cut of the hexahedron, provide a more accurate representation of smooth surface boundary layers. Mixed-element or hybrid meshes currently provide the most optimal meshing solution for very complex moving geometries. Some computational frameworks, such as CREATETM-AV Helios, enable the use of different computational solvers (structured, unstructured, Cartesian) through its multi-mesh, multi-solver paradigm to provide an optimal mesh solution.

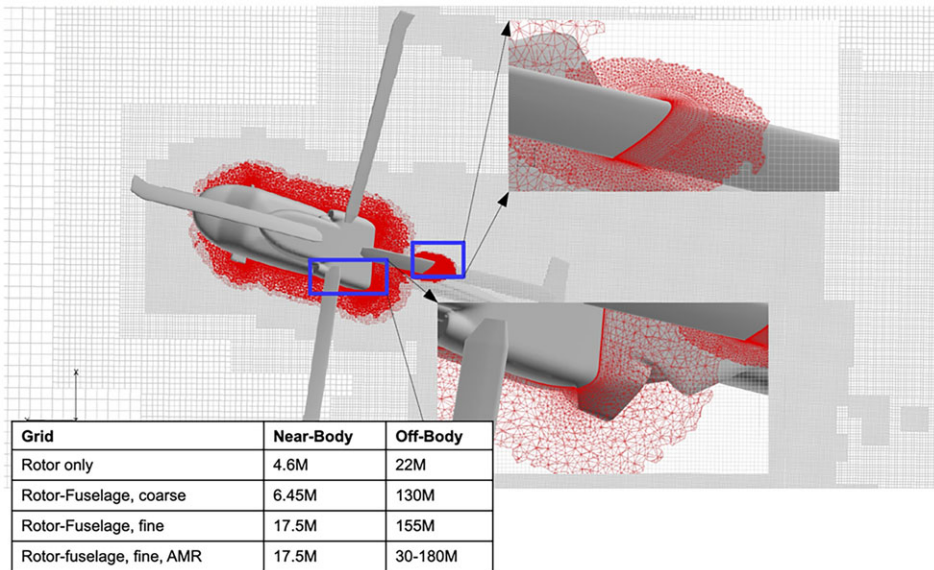


Figure 5. Illustration of a modern complex unstructured, overset mixed-element Helios mesh about a UH-60A rotorcraft. Modified from Figure 7 in Roget et al. [34].

Unstructured meshes can simplify the meshing process of complex geometries, while overset meshes can solve the requirement of motion in different frames of reference, as illustrated by the helicopter in Figure 5. The rotating rotor and hub frame is overset with the translating fuselage and off-body frame. The rotor blade mesh in the upper right illustrates an unstructured mixed-element mesh where smooth body separation may occur, applying prisms near the surface and tetrahedrons beyond that region. The complex fuselage geometry is meshed with tetrahedrons that provide a more cost-efficient mesh where bluff-body separation will be present. The farfield or off-body volume domain is composed of a series of overset Cartesian meshes to capture the wake features without the additional computational overhead of body-fitted mesh mathematics. The Cartesian meshes are layered with increasing mesh volume size to ensure that flow features in the near wake are not overly dissipated by the numerical scheme. Example sizes of volume meshes are included. Adaptive mesh refinement (AMR) can be applied to refine the off-body to more accurately capture these wake features. However, AMR can add significant costs to the solution [33], while fixed refinement regions may be more cost-effective to resolve important flowfield features in some simulations.

While unstructured meshes have the ability to rapidly mesh complex bodies, they also come with increased computational memory and time requirements compared to structured meshes of the same size. Structured meshes, which may require many hours to develop complex meshes and usually involve oversetting or piecing together contiguous meshes, are most computationally cost-efficient. In addition, structured mesh solvers can resolve higher-order spatial schemes (fourth, fifth and sixth order are common), while current unstructured mesh solvers are limited to nominally second-order spatial schemes. Therefore, structured solvers that apply higher-order spatial schemes can achieve the same accuracy as second-order schemes with fewer mesh cells, or these higher-order structured solvers can provide more accurate solutions with the same mesh size.

During validation with experimental model papers, the influence of the wind tunnel walls and model support structures must be assessed. The additional meshing requirements of these features can easily require a 150%–200% increase in the volume mesh cell count, depending on the complexity of the structures. In addition, as many of these validation cases involve subscale models, it may be important to consider the presence of laminar to turbulent transition. The mesh may need to be further refined in

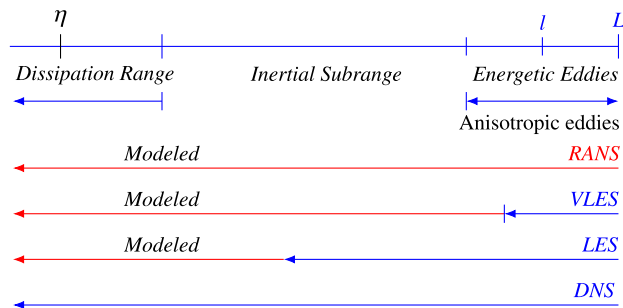


Figure 6. Types of turbulence closures with their ability to capture (blue) or model (red) physical scales of turbulence.

the region of transition (Section 2.3), and the timestep adjusted to accommodate these requirements that may not be present in full-scale applications.

While mesh/solver type is highly dependent on the use case, outcome required, and what solvers are available, best practices should be applied – no matter the application. In particular, novice users should perform literature surveys, to include some of the references listed herein, to determine the best practices for their use case and solver. Mesh and timestep independence studies for new applications are also normal practices by diligent engineers.

2.2 Turbulence closures

Accurate turbulence closures hold the key to successful solutions of separated flows, and they are the primary recipient of the blame when computational solutions do not meet expectations of accuracy, in particular when compared to experimental data. Since the 1970s, researchers have sought more accurate turbulence closures, primarily through the development of models that reproduce the macroscopic effects of turbulence without the need to resolve all spatio-temporal scales. A synopsis of the different types of turbulence closures for the resolution of the Navier-Stokes equations, and their ability to capture or model turbulence scales is illustrated in Figure 6.

Reynolds-averaged Navier-Stokes (RANS) or uRANS solvers model all scales of turbulence. Early algebraic models have given way to one-equation partial differential (PDE) models, which in turn have been replaced by two-equation PDE models for modeling flows with separation. These models have a number of tuning variables, which are typically constants, based on validation problems similar to the character of the problem they are trying to resolve. Various corrections for rotation and limiters on dissipation are common.

A recent study by Sridhar et al. evaluated the influence of two popular versions (Menter and Kok) of the two-equation $k - \omega$ turbulence model [35]. They found that while the two models predicted comparable results for attached flows for configurations that were both moving and static, once separation was introduced, the methods provided similar but different results with all other numerical considerations kept identical. Differences were due to the numerical growth of the turbulent eddy viscosity in the Kok version which also led to numerical instability in some cases. Limiters in the shear stress transport (SST) algorithm added to the Kok model capped the growth, bringing results in line with other models and experiment.

At the other extreme, direct numerical simulations (DNS) attempt to resolve all scales of turbulence within the flowfield. DNS remains a research tool applied to further extend the understanding of the physics within the complex turbulence process. For example, Yeung and Ravikumar [36] further analysed the role of intermittency within turbulence (at low Reynolds numbers) using DNS, which required a mesh of over six trillion mesh points.

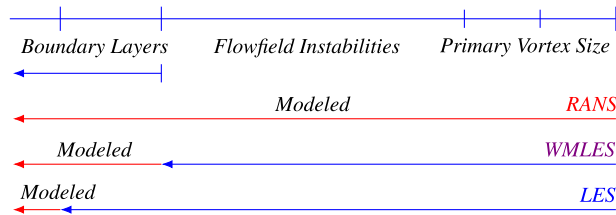


Figure 7. Types of turbulence closures for practical application to separated flows at higher Reynolds numbers.

Large-eddy simulation (LES) provide a compromise between RANS and DNS. LES captures a range of the larger scales of turbulence, based on the mesh size, and model the smaller, less energetic scales. LES simulations with less refined meshes that resolve a smaller subset of the larger turbulence scales is also known as very large LES (VLES). The use of LES can be prohibitively expensive to resolve the very small Kolmogorov scales of turbulence within the boundary layer at larger Reynolds numbers. These very small scales drive the required mesh refinement and timestep size reduction that limit the use of LES for most practical aerospace engineering applications.

To resolve flows where the primary goal is to capture complex features such as separation, researchers have developed innovative solutions – wall-modeled LES (WMLES) – to address the costs of wall-resolved LES, while still retaining much of the accuracy that LES provides. Figure 7 is descriptive of a general definition of these turbulence closures. The characterisation in this figure focuses on the scales of the physical phenomena rather than the turbulence scales which are inherent within the boundary layer.

WMLES has taken on many forms in the past two decades of its primary development. As the boundary layers contain the smallest scales of turbulence, alternatives to LES modeling are applied. Two primary focii have emerged in this endeavour: hybridisation of LES with uRANS and development of wall stress models for LES, similar to those applied for uRANS. For both approaches, the smaller energetic scales of the inner layer (nearest the wall) boundary layer are modeled, using the outer layer LES solution as a boundary condition. Larsson et al. provide a detailed overview of WMLES [37].

In the first approach, the boundary layer – where the smallest, most prohibitive scales of turbulence reside – is modeled with uRANS, while the separated regions are predicted with LES. These hybrid uRANS-LES methods resolve either formal sub-grid scale differential equations for length and turbulent kinetic energy, or the family of detached eddy simulation (DES) approximations [38]. These hybrid schemes may apply either simplified algebraic relations of the length scale or the length scale and eddy viscosity as the trigger between the two methods. Typically, these hybrid approaches evaluate and weight the uRANS or LES/DES option. This has given rise to a number of different switching options between the inner and outer boundary layer zones. Examples of these options include delayed detached eddy simulation (DDES) [39], zonal DES [40] and hybrid RANS-LES (HRLES) [41, 42]. The hybrid uRANS-LES approach has been more widely adopted for use in analyses that involve separation with moving configurations. In particular, the rotorcraft community has adopted this approach as it permits the extension of extant uRANS solutions that include critical capabilities such as multiple reference frames of motion, rotor trim and aeroelastic rotor blades and the CREATETM-AV Helios framework.

The wall-stress modeling approach is similar to the uRANS-LES approach, varying in the solution of the inner layer. The uRANS models typically solve the one- or two-equation differential equations (e.g., Spalart-Allmaras or $k - \omega$ models), while the wall-stress approach assumes equilibrium at the edge of the boundary layer and solves an algebraic form of the eddy-viscosity model.

A question or criticism that occasionally arises with the use of these WMLES methods regards the re-use of RANS meshing and/or timestep in the WMLES simulations. The difference between LES that resolves the boundary layer and these wall-modeling LES approaches is that the smallest scales of turbulence that constrain mesh cell size and timestep are avoided with WMLES. Instead, the mesh in the

Table 1. Predicted characteristics for various turbulence methods and grids for a semi-infinite circular cylinder at $Re = 3,900$. Separation location is given in degrees of azimuth from the leading edge stagnation point. Modified from Lynch and Smith [26].

N_y	Y	Turbulence model	Mean C_D	Strouhal no.	Separation location
–	–	Experiment	0.99 ± 0.05	0.215 ± 0.005 [44]	$86 \pm 2^\circ$ [45]
101	$4D$	$k-\omega$ SST	1.456	0.213	98.4°
51	$4D$	HR-LES	0.971	0.216	85.8°
101	$4D$	HR-LES	0.919	0.217	84.3°
101	$8D$	HR-LES	0.939	0.217	84.7°
48	πD	LES [43]	1.04	0.210	88.0°

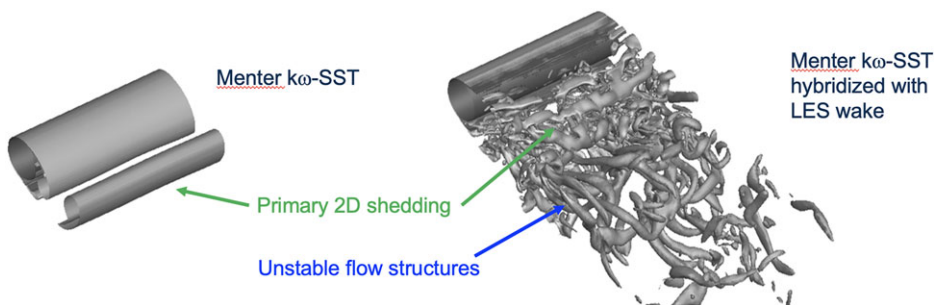


Figure 8. Isocontours of Q -Criterion for a semi-infinite cylinder at $Re=3,900$ at the same mesh (101 span stations) and timestep, from Lynch and Smith [26].

wake, and by extension the timestep, should be appropriate to the larger scales that define the separated flow – usually the size of wake vorticity. Thus the traditional highly refined mesh and timestep sizes of boundary layer LES can be avoided, and best practices associated with the meshes and time-steps for these scales (and uRANS) can be applied. The validity of these assumptions has been demonstrated in a large number of applications, as well as for some canonical LES and uRANS cases.

Lynch and Smith confirmed these assumptions for a semi-infinite cylinder for a wake transitional Reynolds number [26], which is a standard LES test case. Although the cylinder is stationary, its complex wake provides some insight into the development of these methods. The two-equation uRANS model captures the primary shed wake or ‘rollers’ but without any wake artifacts due to the instabilities of the spanwise flow, a phenomenon captured by the WMLES, as illustrated in Figure 8. In addition to the lack of wake refinement, the two-equation uRANS model overpredicts the drag by 50% and the separation location by more than 10 degrees, elucidated in Table 1. Their hybrid uRANS-LES approach was then evaluated for different span extents to examine the spanwise mesh requirements, where the results are within experimental error bounds and comparable to the wall-resolved LES computations of Kravchenko and Moin [43]. The LES wake region acts as a boundary condition for the near-wall uRANS region, which encompassed the cylinder outside the wake and included the attached boundary layer. The LES wake influences and improves the uRANS model, similar to early computational hybrid approaches, such as those that coupled the boundary layer equations with the full potential equations. The centreline pressure distribution around the cylinder confirms this hypothesis in Figure 9. Beyond 60 degrees from the front centreline of the cylinder, the uRANS model underpredicted pressure coefficient (creating a nonphysical region of suction) so that the aft pressure distribution is significantly different from the experiment and the higher-fidelity methods, with a non-physical suction pressure region on the aft portion of the cylinder (Figure 10).

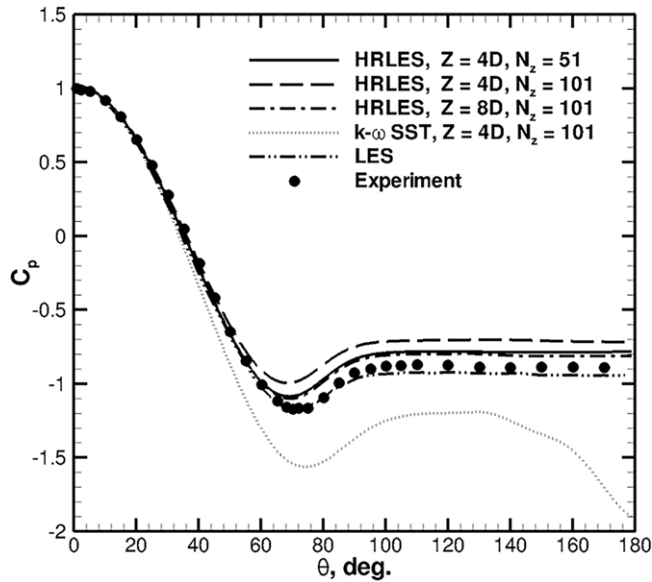


Figure 9. Mean pressure coefficient for the semi-infinite circular cylinder at $Re = 3,900$. Figure 3 from Lynch and Smith [26], including additional data from Krachenko [43].

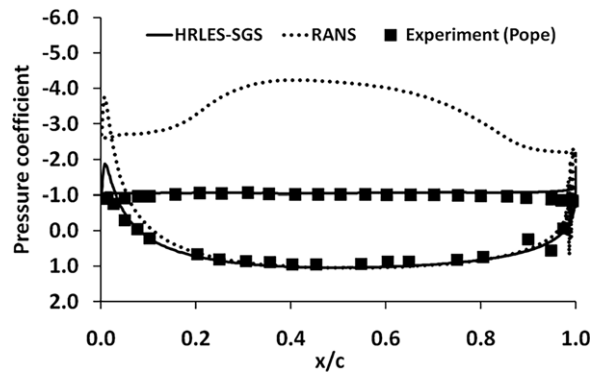


Figure 10. Mean pressure coefficient for a semi-infinite NACA0015 wing at 90° angle-of-attack and $Re = 1,000,000$. From Smith et al. [29].

Smith et al. [29] also confirmed this behaviour for aerofoils at high angles of attack and supercritical Reynolds numbers of one million. The leeward side of the aerofoil, modeled as a semi-infinite wing, exhibits similar underpressure variation with uRANS as the cylinder, while the hybrid RANS-LES approach is able to correctly predict the pressure variation in the separated region, which is key before adding the complexity of unsteady motion.

Hodara et al. extended this evaluation to moving bodies in 2016 [46], applying a different computational solver to a wing in reverse flow. For rotating systems, the addition of forward flight for rotorcraft or yaw for sustainable energy turbines will yield a situation where the local freestream flow starts at the trailing edge and moves towards the leading edge. The artifacts in the shed flowfield can be captured accurately as they emanate from the sharp trailing edge, making this an excellent case study for computations of static and dynamic bodies with separation. Once again, uRANS was insufficient to capture the separation and the shed wake. DDES, which tend to be more sensitive to the mesh and timestep, accurately captured the integrated loads. The details of the wake phenomena were best captured when

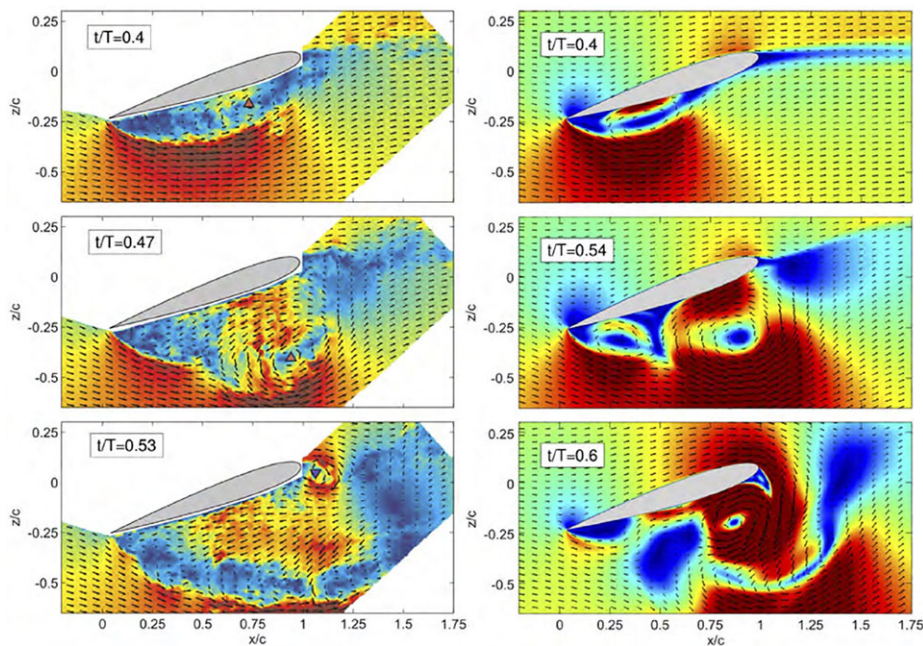


Figure 11. Comparison of the experimental and WMLES-predicted flowfield of a wing undergoing oscillations with separation in a reverse flow [46].

a full subgrid-scale differential equation (here, the turbulent kinetic energy or k equation) was resolved. When modeling these unsteady oscillations, some computational vortices experienced a phase-locked lag in release compared to experiment. These lags occurred only during portions of the oscillation cycle when the flow was separated, illustrated in Figure 11. However, all flowfield features were captured and present when the WMLES turbulence closures were applied. The delay in release of the vortices appeared to be related to the underlying uRANS model and were exacerbated with larger timesteps.

There has also been additional development with traditional LES to make it more tractable for research applications. Implicit scheme LES (ILES) applies larger timesteps than the tradition explicit schemes used by LES. The application of these ILES approaches still have limitations when transition or separation is present, as they may limit the size of the timesteps to maintain stability. The addition of dynamic motion of the vehicle or flowfield can further limit the timestep size. While this approach requires much smaller timesteps than WMLES closures, the introduction of larger CPU or GPU clusters can partially mitigate this time penalty. Using ILES, Visbal [47] was able to evaluate a semi-infinite wing undergoing plunge oscillations at a series of Reynolds numbers where the transition occurred near the leading edge (10,000; 40,000; 60,000). The analysis, which was correlated with experimental data, indicated the presence of complex flowfield primary and secondary structures (Figure 12(a)) similar to those obtained with WMLES (e.g., Figure 8).

A major advantage of the traditional LES (WRLES) approach, in this case ILES, is that these methods are able to accurately capture the dynamic onset of the transition between laminar and turbulent flows, as well as small areas of separation and reattachment, as exemplified in Figure 12(b). However, engineering computations with relevant full-scale Reynolds numbers are still out of reach for most applications.

2.3 Transition models

While traditional LES is able to naturally predict the onset of transition with sufficient mesh resolution in the boundary layer, a reliable transition model for uRANS and WMLES is necessary at higher Reynolds numbers (100,000 and higher) to avoid the high costs associated with smaller turbulence scales

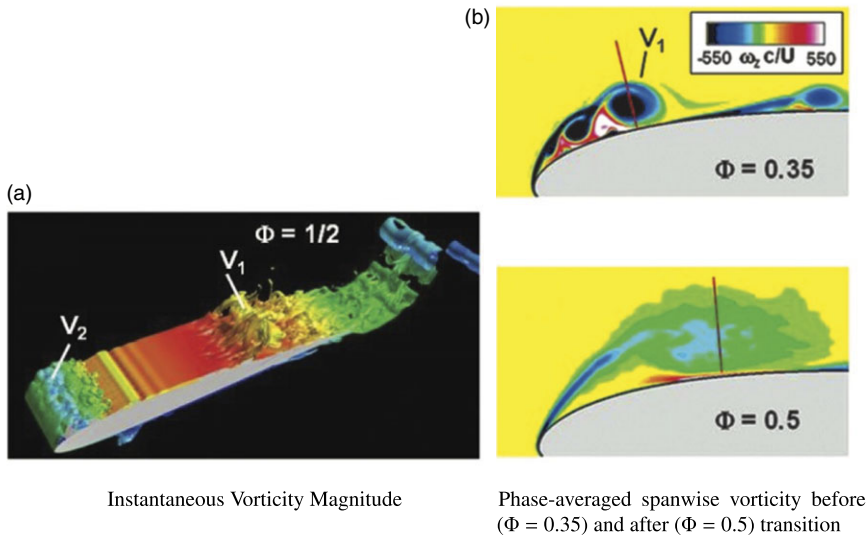


Figure 12. ILES evaluation of a plunging SD7003 aerofoil at a chord-based reduced frequency of $k_f = 3.93$ at a $Re = 40,000$. Φ denotes the location of maximum displacement. Figures modified from Visbal [47].

as Reynolds numbers increase. The ability to predict transition is arguably more important for computational validations with subscale experiments than for many full-scale aerospace applications. Transition modeling, like turbulence models, are often held accountable for otherwise unidentifiable discrepancies between experimental and computational predictions. There are a number of transition models or techniques that can be coupled with uRANS turbulence models and applied in engineering simulations. Two techniques have been applied to uRANS and uRANS-LES approaches with mixed success: the turbulence intensity/momentum thickness (γRe_θ) Langtry-Menter model (LM) and the amplification factor (AFT).

As part of the AIAA Transition Workshop, the LM transition model was applied to several common static test cases [48]. The conclusions noted that while overall the model predicted transition reasonably well, it suffered from freestream turbulence decay, which in turn delayed the onset of transition. In addition, mixed results were obtained with varying grid refinement levels, which appeared to be in part related to the type of transition. Flat plate and strongly attached flows had less success than flows with incipient separation. This latter observation suggests that the LM model could be accurate in flows with more separation and when transition is less influenced by the freestream turbulence.

The AFT model, first developed in 2014, also has many features that are well suited for high performance computing. It is rooted in the local turbulence intensity and the local boundary layer shape factor. Coder earlier assessed the AFT approach using the Spalart-Allmaras (SA) model with the same solver, although most test cases were not the same as the LM assessment [49]. The SA-AFT simulations did not appear to be influenced by freestream turbulence decay, as the onset of transition for these cases was noted to be slightly early compared to experimental data, while the LM model was late. Predictions as angles of attack increased followed this trend. The model at the time of the analysis did not include crossflow corrections, so that transition in flowfields that have strong crossflow components, such as rotating blades and separated wing flows, could less reliably be assessed.

In addition to the ability to correctly predict crossflow in separation, the ability to maintain the Galilean invariance (GI), or proper kinematics across multiple frames of motion, is critical. To date, one of the best efforts to demonstrate the importance of cross-flow and GI is a study of rigid rotors by Jain [33]. He computationally evaluated two rotors with both the LM and AFT models and correlated the results with experimental transition locations identified using differential infrared thermography

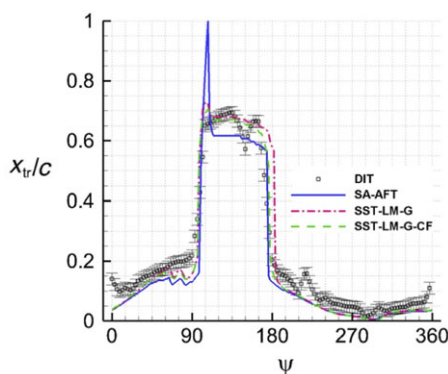


Figure 13. Comparison of the transition predictions with experiment at a radial location of $r/R = 0.85$ for the PSP rotor at $\mu = 0.3$ and $\alpha_s = -3^\circ$, from Jain [33].

(DIT). For both rotors, good agreement is found between the computed and measured transition locations if the transition model includes the GI terms. The influence of cross-flow is more nuanced. The two-dimensional inboard flows at higher blade pitch angles are dominated by the presence of the laminar separation bubbles (LSB), and their prediction is not influenced by the inclusion of the crossflow terms. However, outboard on the rotor, where the finite tip region is dominated by radial flow rather than LSBs, the crossflow terms are necessary to accurately capture the transition locations during a rotor revolution ($0^\circ \leq \psi \leq 360^\circ$). An example of the study results is illustrated in Figure 13 for the pressure-sensitive-paint (PSP) rotor at the $r/R = 0.85$ radius location. The results from the AFT transition model coupled with the Spalart-Allmaras uRANS model (SA-AFT) are typically not as close with experimental results as the results from the Galilean invariant LM model coupled with the $k - \omega$ SST uRANS model (SSTM-LM-G) when compared to experiment (DIT). The SA-AFT also exhibits a sharp peak that needs further exploration to understand its underlying cause. The SST-LM-G predicts a transition location that is farther aft and delayed (later ψ location) than its counterpart with crossflow (SST-LM-G-CF). The additional of crossflow also resulted in larger regions of turbulent flow in the aft rotor disk ($180^\circ \leq \psi \leq 360^\circ$) where the rotor blades can experience separated flows due to interactional aerodynamics.

Overall, these transition models, when applied with best practices, yield predictions that are close to those observed in physical experiments. Two important numerical considerations must be addressed when transition is present. First, the mesh needs to be sufficiently fine on the surface to capture the transition and LSB, if it is present. This usually requires a finer surface mesh than fully turbulent flow assumptions. In addition, the sensitivity of the solution to the numerical scheme types and limiters is also much greater than other computations.

3.0 Applications

The prior sections focused on software and hardware developments during the past two decades that have been critical to understanding key components of predicting separated flows for dynamically moving configurations. This section explores how these developments have advanced or are advancing the understanding of critical applications that involve dynamic, separated flows.

3.1 Dynamic stall

No discussion on the topic of unsteady separated flows would be complete without discussion of dynamic stall. Classic dynamic stall is characterised by an increasing angle-of-attack over time until stall occurs,

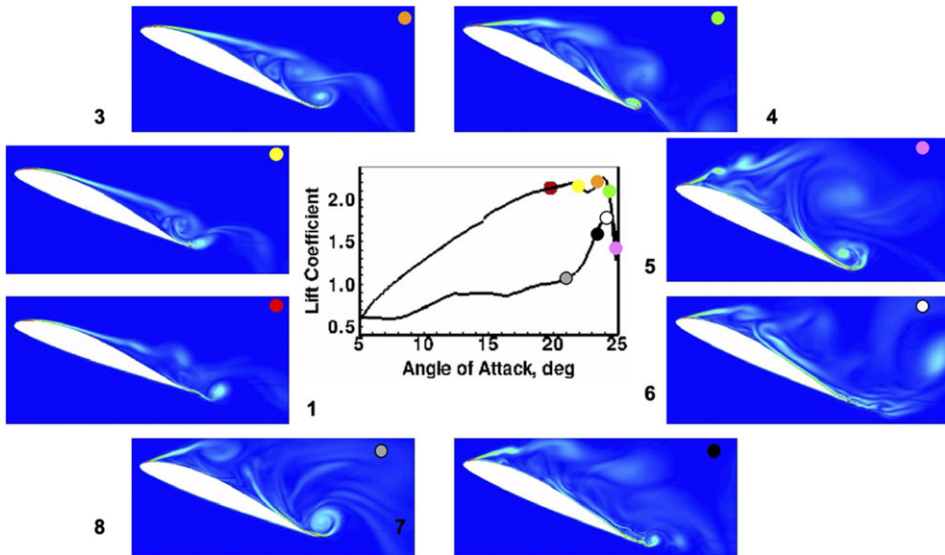


Figure 14. Pictorial definition and flowfields illustrations of classic dynamic stall. Courtesy N. Liggett.

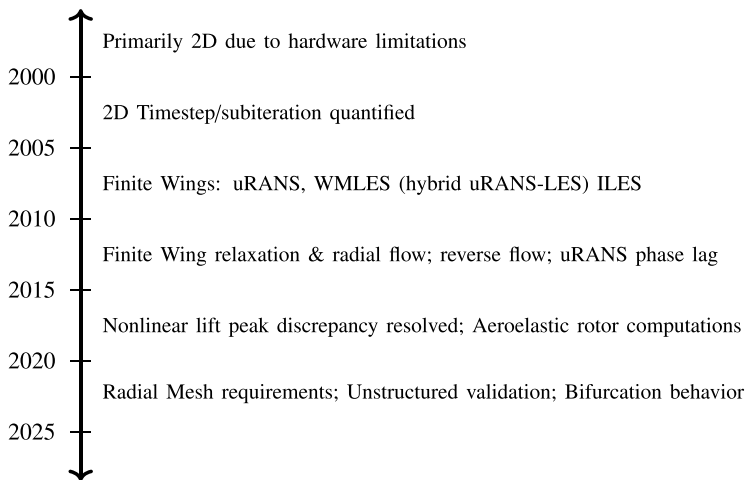


Figure 15. Timeline of dynamic stall computational development, highlighting advances achieved during the past 25 years.

as illustrated in Figure 14. The stall persists as angle-of-attack increases and only recovers when the angle-of-attack is low enough so that the flow can reattach, as is illustrated by the different steps. This definition of dynamic stall is typically attributed to the Carr, McAlister and McCroskey [50]. The angle-of-attack forcing function is oscillatory and can be characterised by a nondimensionalised reduced frequency, $k_f = \frac{\omega b}{V}$. Care must be taken with the k_f parameter, as some aerospace sectors define it with the wing or aerofoil chord, c , rather than the traditional semi-chord ($b = \frac{c}{2}$).

As the efforts to accurately predict dynamic stall computationally span the past 60–70 years (Figure 15), this phenomenon warrants a discussion here. Dynamic stall occurs in fixed-wing flight conditions, for example, fighter aircraft abrupt stall and aeroelastic phenomena such as control surface buzz. It is also prevalent in rotating systems, such as rotorcraft vehicles and wind energy turbines.

Prior to the year 2000, efforts were primarily restricted to two-dimensional applications due to limits in computational hardware. As denoted in Figure 15, major advances parallel the increase in hardware

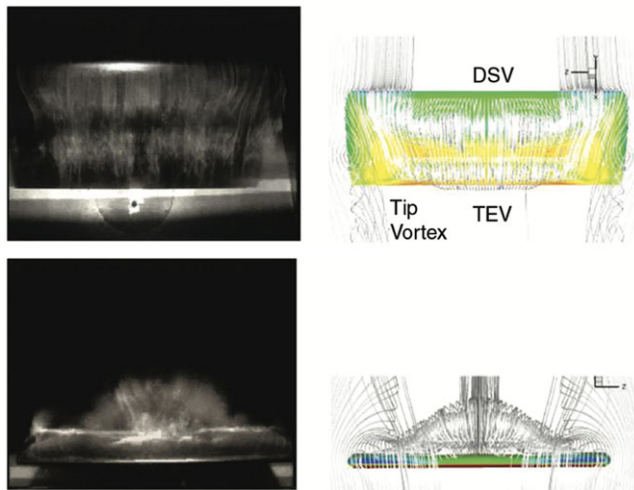


Figure 16. Correlation of computational dynamic stall (right) with experimental smoke visualisation (left) for an aspect ratio 3 NACA0015 wing at a $Re = 13,000$, $M = 0.1$ and a nondimensional pitch rate ($\alpha + = \frac{\dot{\alpha}c}{U_\infty}$) of 0.16. Planform view across the top; leading edge looking aft across the bottom. From Spentzos et al. [54] with experimental data originally from Moir and Coton [55].

and software capabilities. Progress generally, but not always, followed the characterisation of dynamic stall in two dimensions from aerofoils to semi-infinite wings, to finite wings, and then to full vehicles. Dynamic stall is a critical phenomenon in rotorcraft, impacting both vibratory loading and performance, so significant resources have been expended in rotorcraft research to understand, predict, and mitigate dynamic stall.

Computational characterisation of dynamic stall moved from simple aerofoils to semi-infinite wings as computational resources improved. Early efforts focused on improving the accuracy of computationally generated C-81 lookup tables. These tables are applied in blade-element methods that comprise the bulk of the rotorcraft engineering analyses [51]. The modeling of three-dimensional semi-infinite computational domains was an important advancement since turbulence and separation are three-dimensional phenomena. Computational validations had previously been performed with experimental campaigns that evaluated simple geometries (wall-to-wall rectangular wings of a single aerofoil). Those correlations indicated that the aerodynamic coefficients of the experiments exhibited significant three-dimensional relief effects that were not present in the uRANS-predicted aerodynamic coefficients. When semi-infinite computations were performed, the aerodynamic coefficients more accurately represented the mean cyclic behaviour of the experiments. Both two- and three-dimensional studies identified best practices for the timestep and mesh requirements for dynamic stall [29, 52].

Concurrent with and following these studies, finite wings undergoing dynamic stall were also being computationally evaluated. Spentzos et al. [53, 54] demonstrated the ability of uRANS (two-equation $k - \omega$) computations to capture the arch or omega vortex detected in dynamic stall experiments from numerous sources, including Moir and Coton a decade earlier [55], as illustrated in Figure 16. They also characterised the presence of large radial flows when separation appeared. The latter observation was important as rotorcraft researchers could first study the ability of computational methods to capture radial flows during fixed-wing dynamic stall without adding more complex and costly rotation.

These early efforts were followed by further evaluations on oscillating finite wings using uRANS [56–58], WMLES [57, 59] and LES [60]. A series of evaluations by the rotorcraft community were correlated with experimental data for the OA205 finite wing with an aspect ratio of 3 and a Reynolds number of 1 million for static and dynamic stall [61]. Kaufmann et al. confirmed the ability for uRANS to capture the omega vortex [56]. Richez et al. [57] found that uRANS was not able to capture many of the important

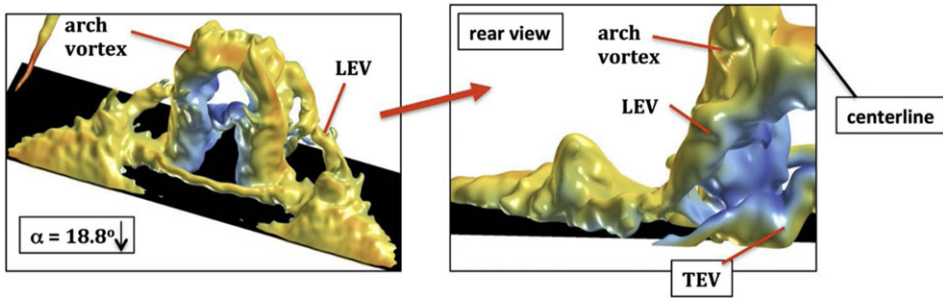


Figure 17. Illustration of the omega vortex interactions during dynamic stall on a pitching NACA0012 aspect ratio 4 wing evaluated with ILES for $M_\infty = 0.1$ and $Re_c = 200,000$. Modified from Visbal et al. [60].

underlying physics, but their WMLES was able to capture them. Jain and his collaborators evaluated the OA205 finite wing with different solvers and uRANS and WMLES (DDES) for both static and dynamic stall [59]. They confirmed the earlier observations of radial flows in dynamic separation, and, at the Reynolds number evaluated ($Re = 1 \times 10^6$), that transition models improved the airload accuracy prediction when correlated to experiment. They evaluated both light (small zones of separated flow) and deep (large areas of separated flow) dynamic stall, indicating that when the best practices adopted from the semi-infinite two-dimensional computational studies were applied, the computational approaches predicted both types of dynamic stall well.

Air Force Research Lab (US) researchers studied finite wing dynamic stall at lower Reynolds numbers ($Re = 200,000$) with their ILES solvers [60]. In this work, they were able to computationally characterise the influence of aspect ratio and wall mounting. The character of the arch or omega vortex was investigated for various scenarios, confirming the earlier findings with uRANS and WMLES. Although computed at lower Reynolds numbers and currently too costly for engineering analyses, the LES analyses are exceptionally valuable in further elucidating the details and importance of the physical phenomena during the dynamic stall. Some phenomena drive accurate airloads, while others may be less important. An example is the development of the omega or arch vortex, depicted in Figure 17. While all approaches have captured the macroscale vortex, the developmental details and strength of the vortex that require much smaller scales can be studied with these LES simulations. The importance of the developmental features then drive the mesh, timestep, transition and turbulence details of the approaches with additional modeling assumptions.

Another application that has relevance to dynamic stall and aeroelasticity is the motion of control surfaces with respect to a wing that is either static or moving itself. In this exemplar study, the use of a WMLES turbulence closure ($k - \omega$ uRANS with k -equation LES subgrid-scale model), combined with overset meshes in relative motion, illustrates the importance of modeling details such as the gaps between the flaps [30, 31]. Computational evaluations were performed with both a separate flap that included the gap and an integrated flap that did not include the gap. In this study, a NACA0012 wing at $M_\infty = 0.4$, $Re = 1.6M$ and $\alpha = 4^\circ$ included a flap oscillating at a reduced frequency, $k_f = 0.042$ while the aerofoil oscillated at $k_f = 0.021$. The flowfield variation during one cycle of the flap oscillation (Figure 18(a)) illustrates some of the complex interactions that occur within the gap. The influence of modeling these gap interactions is clearly observed in integrated aerodynamic variables. Lift coefficient is the exemplar variation in Figure 18(b), though similar trends are observed with drag and pitching moment. While the overall trends are captured with an integrated flap, the predicted magnitudes of the coefficients can be larger than the modeled gap results and experiment [62]. The gap provides a relief effect that, with the WMLES turbulence closure accurately follows the experimental results.

Advances in the accuracy of high-quality computational data over the past two decades in particular have spurred improved and concurrent collaboration with experimentalists. For example, the traditional experimental practice provided a single point per timestep for an analysis, typically time-averaged, or

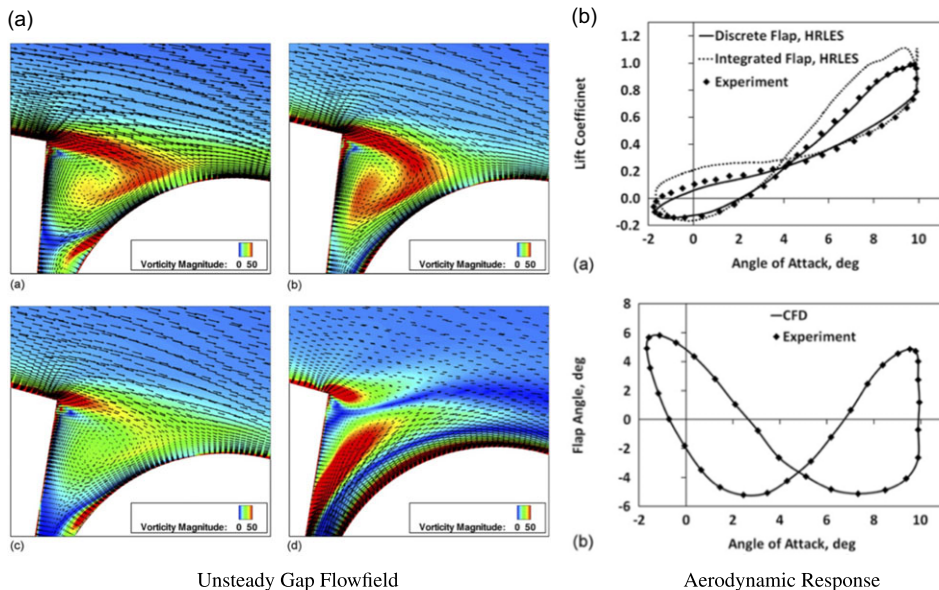


Figure 18. Computational simulations of an oscillating NACA0012 aerofoil-flap semi-infinite wing at $M_\infty = 0.4$ and $Re_\infty = 1.63$ million. The main aerofoil oscillates about $\alpha_{\text{mean}} = 4^\circ \pm 6^\circ$ at $k_f = 0.021$. The flap oscillates about $\alpha_{\text{mean}} = 0^\circ \pm 6^\circ$ at $k_f = 0.042$. From Liggett et al. [30].

if periodic, phase averaged is no longer sufficient. In some instances, error bars associated with the instrumentation uncertainty have been provided. More recent experimental campaigns [63–65] provide either mean data with standard deviation bounds or unsteady min/max extents of the measured variable over many oscillations to provide an estimate of ‘what is good enough’ to for computational validation.

Recognition of the unsteadiness during experimental campaigns associated with these unsteady flowfields is not a new observation. Carr, McAlister and McCroskey observed the presence of flow variations in their now classic 1977 NASA Technical Note [50]. Experimentalists deduced these effects from ‘random turbulent fluctuations’ or other sources by phase averaging over many cycles.

In some instances, this phase averaging can lead to erroneous or biased data. One example of this is associated with dynamic stall. Computational results of integrated aerodynamic coefficients consistently indicated a stronger nonlinear lift peak generated by the leading edge vortex just prior to stall over their experimental counterpart. These differences could not be explained through mesh and time-step refinements, three-dimensional effects, or advanced turbulence models. Ramasamy et al. [66] undertook a more detailed analysis of recent experiment data and established that phase averaging of the data smoothed a slight aperiodicity in lift peak, introducing a bias in the data and reducing the magnitude of the nonlinear lift peak. Recent efforts by Ramasamy et al. [67] identified using cycle-to-cycle experimental data that dynamic stall can include one or more furcations associated with different physics present in a cycle. These different modalities may be caused by a number of physical phenomena, including but not limited to variations in the separation location, leading edge or trailing edge stall onset, presence of dynamic stall vortices, and time of reattachment angle. Test conditions (wall conditions, flow aperiodicity, random turbulence fluctuations) may also induce cycle-to-cycle variations, where phase averaging can introduce bias or erroneous conclusions.

Tran et al. [68] further explored this behaviour using both experimental and computational results. Figure 19(a) elucidates the bimodal behaviour with the previous experimental data from Ramasamy et al. [67]. Cluster 1 in blue indicates cycles with a dynamic stall, while cluster 2 cycles in red do not have a stall event. As cluster 2 dominates the experiment for 87% of the time, phase averaging of all of the data cycles (black line) indicates that dynamic stall is not present, leading to an erroneous conclusion.

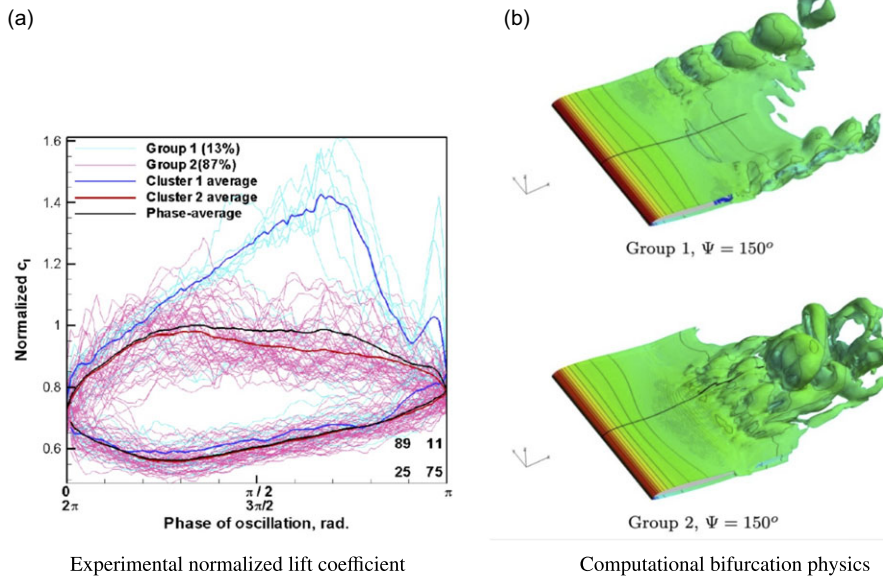


Figure 19. Variational cycle-to-cycle cluster comparison in dynamic stall for a modified VR-12 aerofoil at $\alpha = 18^\circ \pm 5^\circ$, $M_\infty = 0.3$, $k_f = 0.10$, from Tran et al. [68] and experimental data from Ramasamy et al. [67].

The authors also performed a computational analysis with Helios, over many cycles with refined temporal analysis and WMLES-based turbulence models (DDES). These computations reproduced these bifurcations with excellent accuracy, though the overall combined analysis resulted in some differences as the computations reported different weighting of each cluster compared to its experimental counterpart. This collaboration was key as the computational results provided additional flowfield insights to aid in the explanation of the phenomena driving these variations (Figure 19(b)). Detailed collaborative analyses such as these are providing new insights into these complex separated flows.

The costs of the simulations discussed thus far are very prohibitive, so active research is ongoing to develop methods that provide the same accuracy for aeromechanics at significantly reduced computational time. Hybrid solvers, applied via bespoke coupling algorithms or within frameworks such as Helios, apply the very costly refined viscous simulations near the body to capture the separation, shear layers and vorticity on the body. The mid- and far-field are resolved using potential-based solvers. These second-generation methodologies correct earlier limitations with boundary conditions, simple geometries (i.e., a single rotor blade), and turbulence modeling. The most successful of these hybrid solvers include free-wake methods [69–72] and velocity-vorticity wake formulations [73–75]. Researchers developing the free-wake coupling report comparable uRANS accuracy (within 2% – 5%) for aerodynamic (and structural dynamics) loads for rotors, with 50% and 90% reduction in computational costs for flight conditions with dynamic stall and attached flows, respectively. The reduction in costs is two-fold with a reduction in mesh requirements and a more rapid convergence of the wake. A recent addition to the Helios suite, the reduced order aerodynamics model (ROAM) is another option to address the high cost associated with high-fidelity CFD simulation, in particular for rotorcraft design. ROAM applies an actuator line model for the rotor(s), while non-lifting bodies (fuselage, nacelles, etc.) are resolved via an immersed boundary method [76]. A wall model, detailed in Jude et al., [77] was recently added that improved flowfield predictions and better correlation with high-fidelity results for separated flows.

These are but a few highlights of the advances over the past quarter century in dynamic stall. Overviews of progress in the computation and understanding of dynamic, separated rotorcraft flows

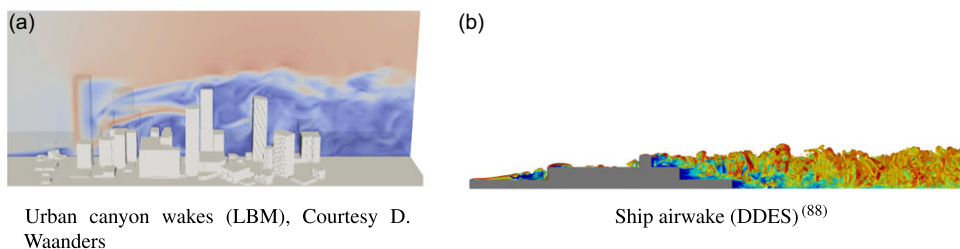


Figure 20. Computational examples of the variation of the winds in the wakes of obstacles.

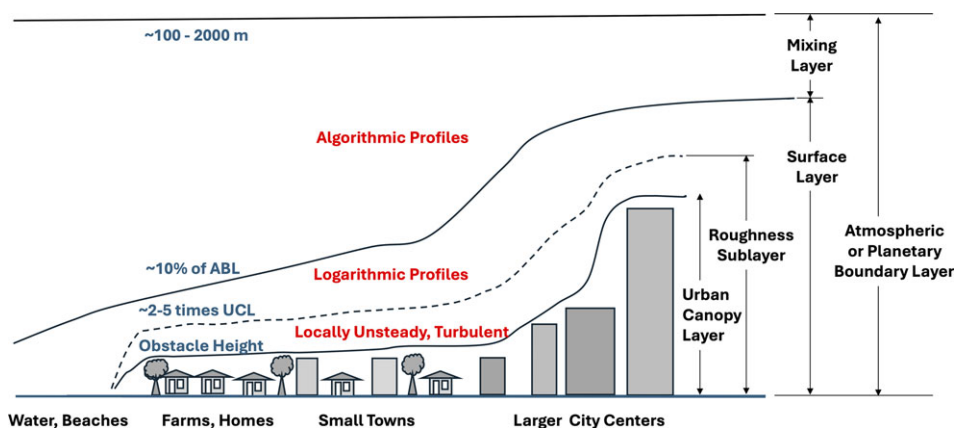


Figure 21. A representative schematic of the atmospheric boundary layer where AAM and UAV flight paths will be, from Salins et al. [90].

can be found in Yeo and Ormiston [78, 79], van der Wall et al. [80], Smith et al. [81], Smith et al. [82, 83], Gardner et al. [65] and Smith [84], in addition to individual publications. By applying the software and hardware advances highlighted in Section 2 and the extant literature, the understanding of and ability to computationally predict a complex dynamic phenomenon, dynamic stall, has been significantly advanced over the past quarter century.

3.2 Aerodynamics of transient environments

Another area of emerging critical importance in this area is vehicle interaction with intense and sometimes large transients that are encountered in airwakes near obstacles, such as in urban environments and ship airwakes illustrated in Figure 20. Flight in these unsteady airwakes has implications for military and civilian use cases from very small uncrewed air vehicles (UAV) to advanced air mobility (AAM) to traditional full-size rotorcraft. Flight through these environments affects flight safety [85], pilot workload, passenger ride quality and operational life cycle and maintenance of vehicles [86]. Operations near heliports/vertiports in an obstacle-rich area can pose significant safety hazards to nearby nonparticipants [87].

Traditionally, engineers have applied indicial theory or considered gusts that remain relatively small compared to the forward flight speed of the air vehicles. However, this is not the case when vehicles operate in the roughness sublayer (RL) of the atmospheric boundary layer (ABL), per Figure 21. In the RL, flight vehicles will rapidly encounter a changing environment composed of shear layers, shed vortices, and recirculation zones that will create equivalent transverse and streamwise gusts [89].

Of similar interest are shipboard rotorcraft flight operations, where the atmospheric boundary layer drives the turbulent environment around the ship so that flight deck operations occur in a highly transient

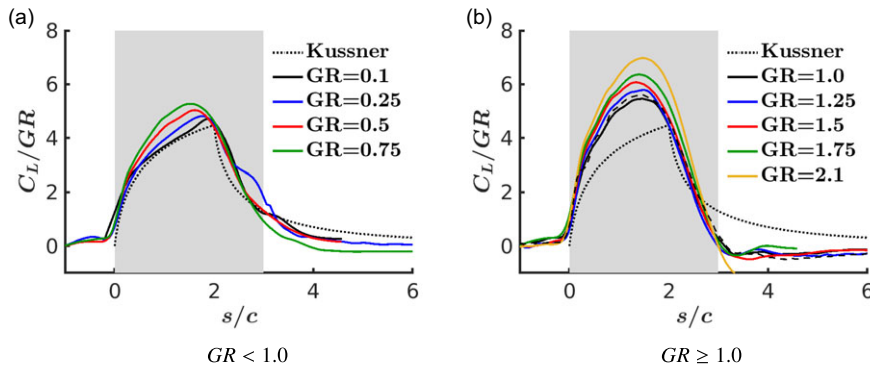


Figure 22. Wing-gust lift response with increasing gust ratio [91]. Experimental data [92] for $GR = 1$ is presented as a dashed line.

environment (Figure 20(b)). The pilot workload and operational safety can be adversely impacted both in forward flight and hover.

During the past decade, experimental and computational groups have been collaboratively investigating these gusts and environments to gain an understanding of the physics and develop the best computational practices for flight through them [89]. For example, for transverse gusts interacting with lifting surfaces above gust ratios of 0.5–0.75, there is a distinct change in the physics and, correspondingly, the aerodynamic behaviour compared with lower gust ratios (Figure 22), the response can be accurately predicted with Küssner indicial theory as the interaction is linear. As the gust ratio increases, there is an interaction of the leading and trailing edge vortices, along with significant flow separation, so that the overall aerodynamic interaction is nonlinear and linear indicial theory is no longer accurate.

Current research efforts are ongoing to explore different kinds of unsteady turbulent interactions, how shapes and extents of transients influence the vehicle behaviour, how to predict and model the transients and how to prevent adverse impacts of flight through these transients. Much of the early research focused on the resolution of the physics for fixed lifting surfaces – that is, the gust interacts with the lifting surface, but the surface does not move in response to the gust interaction. For heavy vehicles with significant inertia these assumptions may be good approximations, but as vehicle weight decreases, these are not valid assumptions. A 10 kg UAV and Blackhawk helicopter will respond quite differently to the same gust ratio. The full gust velocity may be absorbed by the larger Blackhawk vehicle, with little uncommanded vehicle displacement. However, the light UAV will respond to the gust velocity primarily through vehicle displacement, so that the effective gust ratio is reduced [93, 94]. Therefore, the inclusion of flight controls and/or rigid body modes need to be considering during computational evaluations of these interactions.

The computational modeling of these interactional flows pose some different issues than those previously discussed for dynamic stall. These interactions are not periodic, but pose a single, unique transient. Thus, while for periodic flows the simulation can include many different cycles of the behaviour to ensure accuracy and study the unsteady details, that is not possible here. A practical approach to these computational assessments is the use of overset grids to ‘fly’ the vehicle or lift component through the unsteady environment. For uRANS, WMLES and LES applications, ensuring that Galilean invariance (GI) of the models is maintained is crucial. To illustrate this, a spanwise station of a lifting surface interacting with a transverse gust at a transitional Re is examined in Figure 23. When the simulation involves a traditional single frame of reference with the aerofoil velocity modeled as an inflow variable as in Figure 23(b), if grid motion (or an overset mesh) does not include GI in the LM transition model, an incorrect flowfield results (Figure 23(a)). The correct flowfield is recovered when the GI terms in the LM model are added (Figure 23(c)). This simple example shows the importance of understanding the numerical implication of moving frames of motion.

With bodies experiencing these transient conditions, where the unsteadiness is not caused by body motion, maintaining convergence and solution accuracy is dependent on the situation and the solution

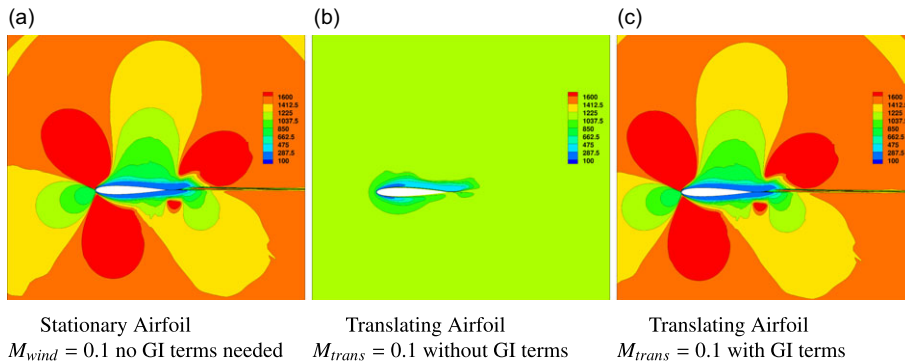


Figure 23. \tilde{Re}_{0t} field for stationary and translating NACA0012 aerofoil, from Crawford [95].

may become unstable using nominally best convergence practices from periodic simulations [95]. For these gusts, for example, the simulation accuracy is dependent on achieving temporal convergence prior to the gust interaction. For changing inflows, such as flight through an urban canyon, the numerical convergence should be monitored during the unsteady simulation, and, if required, numerical options modified to ensure an accurate, stable solution. It was also observed that gust solutions are less accurate when dissipative first-order schemes are applied to improve solution stability [95]. Traditional measures of convergence in separated flows, typically two orders of magnitude reduction, may not be sufficient in these scenarios. This is an area of ongoing research and development.

The simulation of an unsteady environment through the solution of the Navier-Stokes (N-S) equations is problematic due to the dissipative nature of the computational representation of the N-S equations. If a boundary condition is used to impress an unsteady, changing environment, the velocity and vorticity inputs may fully or significantly disappear when they reach the configuration under analysis. There have been various approaches to mitigate this problem using multiple solvers [70] and jets to model gusts [91], for example. Wales et al. [96] introduced a more generic approach to model these unsteady conditions without encountering dissipation. Similar to the additional terms that are added for moving grids, additional source terms that propagate the unsteady conditions can be added to the numerical solver. When properly modified, the solver is able to provide a two-way coupling or interaction where the unsteady environment is felt on the vehicle and the vehicle effects modify the environment. In larger transients and gusts, this nonlinear interaction is important in accurately capturing the physics [89, 94, 97].

4.0 Current and future prospects

While there have been major advances over the past quarter century since Elsenaar's 2000 Lanchester lecture [15], there are current and emerging research areas that promise further significant achievements to progress this field over the next 25 years.

Lattice-Boltzmann Methods: Development of alternative methods that can provide the accuracy of the solution of the uRANS equations but at significantly reduced costs is a significant area of interest. The hybrid solvers discussed earlier have had good success but cost reductions of several orders of magnitudes are sought to make these more tractable for engineering analysis, modeling and simulation (M&S), and design. One such alternative is the lattice Boltzmann method (LBM) as an approach to replace uRANS for some use cases. Progress has been made in the use of LBM analyses for real-time dynamic ship airwake assessments [98], as well as positive correlation with experiment and/or uRANS for air wake analyses on ships [88, 99] and urban environments [100]. These applications succeed as the flowfields are dominated by fixed-point separations at well-defined sharp corners. LBM methods at mid-fidelity resolution levels cannot accurately capture the near-wall viscous phenomena that arise

on the vehicle or obstacle without substantial mesh and timestep refinement required to capture these smaller-scale phenomena. Additional research in wall modeling techniques to alleviate these restrictive requirements is a topic that can have a significant impact on the usefulness of LBM in aerodynamics.

Machine Learning Techniques: The uRANS or LBM computational simulations for separated flows produce terabytes of data as researchers explore and categorise the important physics. This large amount of data can become a bottleneck in understanding what variables influence the complex flow and aerodynamic loads. Prior research has demonstrated that automatic mesh refinement (AMR) can aid in defining the solution sensitivities and refining important flowfield characteristics [59, 101]. AMR can be very expensive and some approaches require *a priori* knowledge of the important variables and necessary levels of refinement. ML, along with artificial intelligence (AI), is a viable alternative to developing cost effective meshing and identifying the variables driving the solution accuracy.

Machine learning techniques offer an alternative to identify key variables and guide a design of experiments, understand important phenomena or develop reduced-order models. ML also has the potential to inform decision-making algorithms fueled through AI techniques. While there is no indication that ML/AI can reproduce the complex physics in these simulations, ML has recently had substantial success in developing methods to replace aerodynamic coefficient table development for blade element analysis [102] and reproducing the complex flowfield in the wakes of obstacles such as ships [103–105] and urban canyons [100, 106].

In addition, significant improvements to turbulence and transition algorithms can be realised by using ML to replace equation constants as variables that should adapt to the local environment. Some success has been established in the LES community using locally dynamic kinetic model (LDKM) where the subgrid scale changes as needed [107]. Combined with highly localised mesh refinement along with overset meshing, ML can help obviate large mesh requirements. Algorithms that also adapt to locally changing timesteps, working in conjunction with the remainder of the simulation to maintain time accuracy are also a potential area of research. To become a breakthrough, these methods need to be efficient on multiple processors, dynamically interacting with additional or fewer processors as needed.

Uncertainty Quantification and Certification by Analysis: This discourse has specifically avoided opining thus far on the topics of uncertainty quantification (UQ) and ‘certification by analysis’ (CbA). These topics are exceptionally complex and deserve multiple lectures solely on themselves. Certainly UQ is necessary to achieve CbA. UQ be used to identify when a simulation has reached its ultimate use; and to provide the engineering applications that industry demands. This is difficult for dynamic simulations, as researchers have not yet in many instances, defined accuracy with enough sufficiency over the time period of interest, much less quantify the uncertainties and errors. In addition, care needs to be taken with these uncertainty metrics – aleatory and epistemic uncertainties can result in very different outcomes, and if applied incorrectly can provide completely erroneous conclusions.

5.0 Concluding remarks

Dr. Lanchester, in the preface to the 4th edition of his chief oeuvre, *Aerodynamics*: ‘...the study of Aerial Flight will take its place as one of the foremost of the applied sciences, one of which the underlying principles furnish some of the most beautiful and fascinating problems in the whole domain of practical dynamics’ [5].

Even after more than 100 years, this quote reflects that the study of aerodynamics is still of keen interest and importance in aeronautics. The study of aerodynamics has matured to include high-performance computations which now permit significant advances in the resolution of highly unsteady, complex phenomena that were unrealisable even a decade ago. Unlike Dr. Lanchester’s approach, collaboration between multiple computational researchers and computational-experimental efforts are now routine and have resulted in major developments that have benefited the aviation community.

Advances during the past quarter century have revolutionised the field of computational unsteady aerodynamics when separation is present. Major hardware advances with significant investment in

advanced algorithm development and improved experimental validation data have paid significant dividends. Computational methods, when applied with the appropriate meshes and appropriately defined numerical options, can provide accurate predictions of many of the problems the aerospace community faces in the subsonic and transonic flight regimes. One of the largest problems that the community needs to address is that best practices are disseminated, along with the limitations of their applications, to users, and that engineers actually apply them correctly. It is worth noting again this quote from Rogers Lanchester Lecture [14]: ‘The availability of computers does not absolve us from thinking deeply about the fluid-dynamic nature of the problem’. This statement is perhaps even more important today when computational methods proliferate, and many engineers must rely sole on computational results to make engineering decisions.

While some characteristics of aerodynamics are mature, aerodynamics play a key role in many interdisciplinary applications, such as aeroelasticity of lifting and control surfaces; flight safety of pilots, passengers and onlookers; and new use cases such as AAM and UAS or certification by analysis. There still remain significant areas of development where improvements are needed and where research investment is warranted.

A final cautionary observation is warranted for the new generation of researchers. In the 1990s, a major thrust was initiated to replace physical wind tunnels with ‘virtual wind tunnels’ composed of computational fluid dynamics solutions. The concept was highly oversold and resulted in the closure of some test facilities that had been critical to advance aerospace engineering, while the promised computational accuracy and cost effectiveness was never realised. The aerospace engineering community is still recovering from these actions almost 30 years later. While ML and AI will be key in optimising engineering processes both during simulation and analysis, caution should be exercised in asserting that they will replace computational analyses (and physical testing) of these unsteady complex aerodynamics in the next quarter century.

Acknowledgements. The author would like to thank her colleagues and collaborators for their contributions to this publication, in particular Aaron Crawford, Nathan Hariharan, Rohit Jain, Brenden Oates, Pranav Sridhar and Andy Wissink for their valuable comments. She thanks Nicholas Liggett, Aaron Crawford and Duncan Waanders for the use of Figure 14, 23 and 19, respectively. This work would not be possible without the support of many sponsors, in particular the Vertical Lift Research Center of Excellence (VLRCE), Technical Monitor, Mahendra Bhagwat and her many students whose research efforts converted ideas and theories into specific engineering advancements.

References

- [1] Ackroyd, J.A.D. “Lanchester – The Man,” Technical report, Aero. Report 9111, University of Manchester, UK, September 1991.
- [2] Fletcher, J. Frederick William Lanchester, in *The Lanchester Legacy, Vol. 3 – A Celebration of Genius*, Fletcher, J. (Ed), Chap. 2, Coventry University Enterprises Ltd., 1995, Coventry, pp 4–22.
- [3] Kingsford, P.W. F. W. *Lanchester: A Life of an Engineer*, London: Edward Arnold Publishers Ltd., 1960.
- [4] Dawson, J. Patent applications and specifications, in *The Lanchester Legacy, Vol. 3 – A Celebration of Genius*, Fletcher, J. (Ed), Chap. Appendix, Coventry University Enterprises Ltd., 1995, Coventry, pp 246–259.
- [5] Lanchester, F.W. *Aerodynamics*, 4th edn, London: Constable and Company, Ltd., 1918.
- [6] Lanchester, F.W. The flying machine: the aerofoil in the light of theory and experiment, *Proc. Inst. Automobile Eng.*, 1915, **9**, (2), pp 171–259. <https://doi.org/10.1243/PIAEPROC191400901702>
- [7] Prandtl, L. The generation of vortices in fluids of small viscosity: the fifteenth Wilbur Wright memorial lecture, *J. R. Aeronaut. Soc.*, 1927, **1918**, pp 718–741.
- [8] Ackroyd, J.A.D. Lanchester’s aerodynamics, in Fletcher, J. (Ed.), *The Lanchester Legacy, Vol. 3 – A Celebration of Genius*, Chap. 5, Coventry University Enterprises Ltd., 1995, Coventry, pp. 61–98.
- [9] Lanchester, F.W. The Screw Propeller, *Proc. Inst. Automobile Eng.*, 1915, **9**, (2), pp 263–354. <https://doi.org/10.1243/PIAEPROC191400901902>
- [10] Langley, S.P. *Experiments in Aerodynamics*, 2nd edn, Washington, DC: Smithsonian Institution, 1902.
- [11] Smith, M.J. F. W. Lanchester: forgotten contributions to rotorcraft aerodynamic theory and vehicle design,” in *Proceedings of the Vertical Flight Society 80th Annual Forum*, Montréal, Canada, May 7–9, 2024. <https://doi.org/10.4050/F-0080-2024-1369>
- [12] Collar, A.R. Aeroelasticity – retrospect and prospect, *J. R. Aeronaut. Soc.*, 1959, **63**, (577), pp 1–15. <https://doi.org/10.1017/S0368393100070450>

- [13] Jones, W.P. Trends in unsteady aerodynamics, *J. R. Aeronaut. Soc.*, 1963, **67**, (627), pp 137–152. <https://doi.org/10.1017/S0368393100078123>
- [14] Rogers, E.W.E. Aerodynamics — retrospect and prospect, *Aeronaut. J.*, 1982, **86**, (852), pp 43–67. <https://doi.org/10.1017/S0001924000013890>
- [15] Elsenaar, A. Vortex formation and flow separation: the beauty and the beast in aerodynamics, *Aeronaut. J.*, 2000, **104**, (1042), pp 615–633. <https://doi.org/10.1017/S0001924000096858>
- [16] Young, I. Gordon Moore’s Journey: “Moore’s law” Dissected, *IEEE Solid-State Circuits Mag.*, 2024, **16**, (1), pp 42–47. <https://doi.org/10.1109/MSSC.2023.3336168>
- [17] Edwards, C. Moore’s law: what comes next? *Commun. Assoc. Comput. Mach.*, 2021, **64**, (2), pp 12–14. <https://doi.org/10.1145/3440992>
- [18] Nair, R. Evolution of memory architecture, *Proc. IEEE*, 2015, **103**, (8), pp 1331–1345. <https://doi.org/10.1109/JPROC.2015.2435018>
- [19] Dennard, R.H. Field-effect transistor memory, US Patent 3,387,286, June 1968.
- [20] US Department of Defense, DOD High Performance Computing Modernization Program Unclassified Systems, 2022, December 12, 2024. <https://centers.hpc.mil/systems/unclassified.html>
- [21] “The Evolution of HPC,” insideHPC, 2016, December 12, 2024. <https://insidehpc.com/2016/08/the-evolution-of-hpc/>
- [22] Morton, S., McDaniel, D., Sears, D., Tillman, B. and Tuckey, T. Kestrel: a fixed wing virtual aircraft product of the CREATE program, in *47th AIAA Aerospace Sciences Meeting including The New Horizons Forum and Aerospace Exposition*, 5–8 January, Orlando, FL. <https://doi.org/10.2514/6.2009-338>
- [23] Wissink, A., Sitaraman, J., Sankaran, V., Mavriplis, D. and Pulliam, T. A MultiCode Python-Based Infrastructure for Overset CFD with Adaptive Cartesian Grids, in *46th AIAA Aerospace Sciences Meeting and Exhibit*, 7–10 January, Reno, NV. <https://doi.org/10.2514/6.2008-927>
- [24] Sitaraman, J., Katz, A., Jayaraman, B., Wissink, A. and Sankaran, V. Evaluation of a Multi-Solver Paradigm for CFD Using Unstructured and Structured Adaptive Cartesian Grids,” in *46th AIAA Aerospace Sciences Meeting and Exhibit*, 7–10 January, Reno, NV. <https://doi.org/10.2514/6.2008-660>
- [25] Sanchez-Rocha, M., Kirtas, M. and Menon, S. Zonal hybrid RANS-LES method for static and oscillating airfoils and wings,” in *44th AIAA Aerospace Sciences Meeting and Exhibit*, Reno, NV, 2006. <https://doi.org/10.2514/6.2006-1256>
- [26] Lynch, C.E. and Smith, M.J. Extension and exploration of a hybrid turbulence model on unstructured grids, *AIAA J.*, 2011, **49**, (11), pp 2585–2591. <https://doi.org/10.2514/1.56296>
- [27] Palacios, F., Alonso, J., Duraisamy, K., et al. Stanford University Unstructured (SU): An open-source integrated computational environment for multi-physics simulation and design, January 7–10, 2013. <https://doi.org/10.2514/6.2013-287>
- [28] Szydlowski, J. and Costes, M. Simulation of flow around a static and oscillating in pitch NACA0015 airfoil using URANS and DES, in *ASME Heat Transfer Summer Conference*, Charlotte, NC, 2004. <https://doi.org/10.1115/HT-FED2004-56437>
- [29] Smith, M.J., Liggett, N. and Koukol, B.C.G. The aerodynamics of airfoils at high and reverse angles of attack, *J. Aircr.*, 2011, **48**, (6), pp 2012–2023. <https://doi.org/10.2514/1.55358>
- [30] Liggett, N. and Smith, M.J. The physics of modeling unsteady flaps with gaps, *J. Fluids Struct.*, 2013, **38**, (-), pp 255–272. <https://doi.org/10.1016/j.jfluidstructs.2012.12.010>
- [31] Liggett, N. and Smith, M.J. A study of the gap physics of airfoils with unsteady flaps, *J. Aircr.*, 2013, **50**, (2), pp 643–650. <https://doi.org/10.2514/1.C032026>
- [32] Grubb, A. and Smith, M.J. Planform mesh requirements for fixed and rotating wing with separation, *J. Aircr.*, 2025, **62**, (1), pp 132–145. <https://doi.org/10.2514/1.C037859>
- [33] Jain, R. Computational fluid dynamics transition models validation for rotors in unsteady flow conditions, *J. Aircr.*, 2022, **59**, (4), pp 875–895. <https://doi.org/10.2514/1.C036580>
- [34] Roget, B., Sitaraman, J., Wissink, A., Saberi, H. and Chen, W. Maneuvering rotorcraft simulations using HPCMP CREATE™-AV Helios, in *AIAA SciTech Forum, 54th Aerospace Sciences Meeting*, 2016. <https://doi.org/10.2514/6.2016-1057>
- [35] Sridhar, P., Crawford, A. and Smith, M. Sensitivity of rotor aeroelastic predictions with two-equation turbulence models, *CEAS Aeronaut. J.*, 2024, in press. <https://doi.org/10.1007/s13272-024-00797-9>
- [36] Yeung, P.K. and Ravikumar, K. Advancing understanding of turbulence through extreme-scale computation: Intermittency and simulations at large problem sizes, *Phys. Rev. Fluids*, 2020, **5**, (11), p 110517, 21. <https://doi.org/10.1103/PhysRevFluids.5.110517>
- [37] Larsson, J., Kawai, S., Bodart, J. and Bermejo-Moreno, I. Large eddy simulation with modeled wall-stress: recent progress and future directions, *Mech. Eng. Rev.*, 2016, **3**, (1). <https://doi.org/10.1299/mer.15-00418>
- [38] Spalart, P.R., Jou, W.-H., Strelets, M. and Allmaras, S.R. Comments on the Feasibility of LES for Wings, and on a Hybrid RANS/LES approach, in *Proceedings of first AFOSR International Conference on DNS/LES*, Ruston, LA, Greyden Press, Dayton, OH, August 4–8, 1997.
- [39] Spalart, P.R. and Deck, S., Shur, M.L., Squires, K.D., Strelets, M.K. and Travin, A. A new version of detached-eddy simulation, resistant to ambiguous grid densities, *Theor. Comput. Fluid Dyn.*, 2006, pp 181–195. <https://doi.org/10.1007/s00162-006-0015-0>
- [40] Renard, N. and Deck, S. On the interface positioning in a Zonal detached eddy simulation (ZDES) of a spatially developing flat plate turbulent boundary layer, *Progr. Hybrid RANS-LES Model.*, 2015, **130**, pp 203–213.
- [41] Sánchez-Rocha, M. and Menon, S. The compressible hybrid RANS/LES formulation using an additive operator, *J. Comput. Phys.*, 2009, **228**, (6), pp 2037–2062.

- [42] Sánchez-Rocha, M. and Menon, S. An order-of-magnitude approximation for the hybrid terms in the compressible hybrid RANS/LES governing equations, *J. Turbulence*, 2011, **12**, (16), pp 1–22.
- [43] Kravchenko, A.G. and Moin, P. Numerical studies of flow over a circular cylinder at $Re_D = 3900$, *Phys. Fluids*, 2000, **12**, (2), pp 403–417.
- [44] Ong, L. and Wallace, J. The velocity field of the turbulent very near wake of a circular cylinder, *Exp. Fluids*, 1996, **20**, (6), pp 441–453.
- [45] Son, J. and Hanratty, T.J. Velocity gradients at the wall for flow around a cylinder at reynolds numbers 5×10^3 to 10^5 , *J. Fluid Mech.*, 1969, **35**, (2), pp 353–368.
- [46] Hodara, J., Lind, A., Jones, A. and Smith, M.J. Collaborative investigation of the aerodynamic behavior of airfoils in reverse flow, *J. Am. Helicopter Soc.*, 2016, **61**, (2), p 032001. <https://doi.org/10.4050/JAHS.61.032001>
- [47] Visbal, M.R. High-fidelity simulation of transitional flows past a plunging airfoil, *AIAA J.*, 2009, **47**, (11), pp 2685–2697. <https://doi.org/10.2514/1.43038>
- [48] Carnes, J. and Coder, J.G. Benchmarking the Langtry-Menter Transition Model Using OVERFLOW for the AIAA Transition Modeling Workshop, in *AIAA AVIATION 2022 Forum*, June 27 – July 1, Chicago, IL, 2022. <https://doi.org/10.2514/6.2022-3680>
- [49] Coder, J.G. Enhancement of the amplification factor transport transition modeling framework, in *55th AIAA Aerospace Sciences Meeting*, 9–13 January, Grapevine, TX, 2017. <https://doi.org/10.2514/6.2017-1709>
- [50] Carr, L.W. and McAlister, K.W. and McCroskey, W.J. Analysis of the development of dynamic stall based on oscillating airfoil experiments, Technical report, NASA- TN-D-8382, 1977.
- [51] Smith, M.J., Wong, T., Potsdam, M., Baeder, J. and Phanse, S. Evaluation of CFD to determine two-dimensional airfoil characteristics for rotorcraft applications, *J. Am. Helicopter Soc.*, 2006, **50**, (1), pp 70–79. <https://doi.org/10.4050/1.3092879>
- [52] Szydlowski, J. and Costes, M. Simulation of flow around a static and oscillating in pitch NACA0015 airfoil using URANS and DES, in *Proc. ASME Heat Transf./Fluids Eng. Summer Conf. 2004*, **2 B**, Charlotte, NC, July 2004, pp. 891–908. <https://doi.org/10.1115/HT-FED2004-56437>
- [53] Spentzos, A., Barakos, G., Badcock, K., Richards, B., Wernert, P., Schreck, S. and Raffel, M. Investigation of three-dimensional dynamic stall using computational fluid dynamics, *AIAA J.*, 2005, **43**, (5), pp 1023–1033. <https://doi.org/10.2514/1.8830>
- [54] Spentzos, A., Barakos, G.N., Badcock, K.J., Richards, B.E., Coton, F.N., Galbraith, R.A.M., Berton, E. and Favier, D. Computational fluid dynamics study of three-dimensional dynamic stall of various planform shapes, *J. Aircr.*, 2007, **44**, (4), pp 1118–1128. <https://doi.org/10.2514/1.24331>
- [55] Moir, S. and Coton, F. An examination of the dynamic stalling of two wing planforms, Technical Report Aerospace Engineering Rept. 9526, Univ. of Glasgow, Glasgow, Scotland, U.K., 1995.
- [56] Kaufmann, K., Costes, M., Richez, F., Gardner, A. and Le Pape, A. Numerical investigation of three-dimensional static and dynamic stall on a finite wing, *J. Am. Helicopter Soc.*, 2015, **60**, (3), p 032004 (1–12). <https://doi.org/10.4050/JAHS.60.032004>
- [57] Richez, F., Le Pape, A. and Costes, M. Zonal detached-eddy simulation of separated flow around a finite-span wing, *AIAA J.*, 2015, **53**, (11), pp 3157–3166. <https://doi.org/10.2514/1.J053636>
- [58] Kaufmann, K., Merz, C. and Gardner, A.D. Dynamic stall simulations on a pitching finite wing, *J. Aircr.*, 2017, **54**, (4), pp 1303–1316. <https://doi.org/10.2514/1.C034020>
- [59] Jain, R., Le Pape, A., Grubb, A., Costes, M., Richez, F. and Smith, M.J. High-resolution CFD predictions for the static and dynamic stall of a Finitespan OA209 wing, *J. Fluids Struct.*, 2018, **78**. <https://doi.org/10.1016/j.jfluidstructs.2017.12.012>
- [60] Visbal, M.R. and Garmann, D.J. Dynamic stall of a finite-aspect-ratio wing, *AIAA J.*, 2019, **57**, (3), pp 962–977. <https://doi.org/10.2514/1.J057457>
- [61] Le Pape, A., Pailhas, G., David, F. and Deluc, J.-M. Extensive wind tunnel tests measurements of dynamic stall phenomenon for the OA209 airfoil including 3D effects, in *33rd European Rotorcraft Forum 2007, Kazan, Russia*, Curran Associates, Red Hook, NY, 1, 2007, pp. 320–335.
- [62] Krzysiak, A. and Narkiewicz, J. Aerodynamic loads on airfoil with trailing-edge flap pitching with different frequencies, *J. Aircr.*, 2006, **43**, pp 407–418. <https://doi.org/10.2514/1.15597>
- [63] Gardner, A., Richter, K., Mai, H., Altmikus, A., Klein, A. and Rohardt, C.-H. Experimental investigation of dynamic stall performance for the EDI-M109 and EDI-M112 airfoils, *J. Am. Helicopter Soc.*, 2013, **58**, (1), pp 1–13. <https://doi.org/10.4050/JAHS.58.012005>
- [64] Harms, T., Nikoueeeyan, P. and Naughton, J.W. An experimental evaluation of cycle-to-cycle variations of dynamic stall, in *AIAA Aerospace Sciences Meeting*, January 8–12, 2018. <https://doi.org/10.2514/6.2018-1267>
- [65] Gardner, A.D., Jones, A.R., Mulleners, K., Naughton, J.W. and Smith, M.J. Review of rotating wing dynamic stall: experiments and flow control, *Prog. Aerosp. Sci.*, 2023, **137**, p 100887. <https://doi.org/10.1016/j.paerosci.2023.100887>
- [66] Ramasamy, M., Wilson, J.S., McCroskey, W.J. and Martin, P.B. Measured characteristics of cycle-to-cycle variations in dynamic stall,” in *AHS Technical Meeting on Aeromechanics Design for Vertical Lift*, Curran Associates, Red Hook, NY, January 20–22, 2016.
- [67] Ramasamy, M., Sanayri, A., Wilson, J., Martin, P., Harms, T., Nikoueeeyan, P. and Naughton, J. Data-driven optimal basis clustering to characterize cycle-to-cycle variations in dynamic stall measurements, in *Presented at AHS Forum 75, Philadelphia, PA*, Curran Associates, Red Hook, NY, May 2019, pp. 1075–1102.

- [68] Tran, S.A., Sitaraman, J. and Ramasamy, M. Lessons Learned from a Combined Experimental-Computational Study on Pitching Airfoil Cycle-to-cycle Variations, in *AIAA SCITECH Forum*, San Diego, CA, January 3–7, 2022. <https://doi.org/10.2514/6.2022-2414>
- [69] Quon, E.W., Smith, M.J., Whitehouse, G.W. and Wachspress, D.A. Hierarchical variable fidelity methods for rotorcraft aerodynamic design and analysis, in *Proceedings of the American Helicopter Society 67th Annual Forum*, Virginia Beach, VA, Curran Associates, Red Hook, NY, May 3–5, 2011, pp. 362–374.
- [70] Wilbur, I., Moushegian, A., Smith, M.J. and Whitehouse, G. UH-60A rotor analysis with an accurate dual-formulation hybrid aeroelastic methodology, *J. Aircr.*, 2019, **57**, (1), pp 113–127. <https://doi.org/10.2514/1.C035467>
- [71] Moushegian, A. and Smith, M.J. Physics and accuracy of dual-solver simulations of rotors in ground effect, *J. Am. Helicopter Soc.*, 2023, **68**, (1), p 16. <https://doi.org/10.4050/JAHS.68.012010>
- [72] Moushegian, A. and Smith, M.J. A dual-solver hybrid computational approach to integrated propulsion aerodynamics, *J. Aircr.*, 2023, **60**, (2), pp 1–12. <https://doi.org/10.2514/1.C036808>
- [73] Brown, R.E. and Line, A.J. Efficient high-resolution wake modeling using the vorticity transport equation, *AIAA J.*, 2005, **43**, (7), pp 1434–1443. <https://doi.org/10.2514/1.13679>
- [74] Whitehouse, G.R., Silbaugh, B.S. and Boschitsch, A.H. Improving the performance and flexibility of grid-based vorticity-velocity solvers for general rotorcraft flow analysis, in *Proceedings of the 71st Annual Forum of the American Helicopter Society*, Virginia Beach, VA, 2015. <https://doi.org/10.4050/F-0071-2015-10086>
- [75] Whitehouse, G. and Boschitsch, A. Investigation of grid-based vorticity-velocity large eddy simulation off-body solvers for application to overset CFD, *Comput. Fluids*, 2021, **225**, p 104978. <https://doi.org/10.1016/j.compfluid.2021.104978>
- [76] Wissink, A., Jude, D., Jayaraman, B., et al. New capabilities in CREATE™-AV helios version 11, *AIAA Scitech 2021 Forum*, 2021. <https://doi.org/10.2514/6.2021-0235>
- [77] Jude, D., Hosseini, S., Sitaraman, J., Peron, S. and Bolsard, R. Actuator line and immersed boundary methods for rotorcraft CFD, in *80th Forum of the Vertical Flight Society*, May 2024. <https://doi.org/10.4050/F-0080-2024-1128>
- [78] Yeo, H. and Ormiston, R.A. UH-60A Airloads workshop—setting the stage for the rotorcraft CFD/CSD revolution, Part I: background and initial success, *J. Am. Helicopter Soc.*, 2022, **67**, pp 1–17. <https://doi.org/10.4050/JAHS.67.022011>
- [79] Yeo, H. and Ormiston, R.A. UH-60A Airloads workshop—setting the stage for the rotorcraft CFD/CSD revolution, Part II: ongoing progress, impact, and lessons learned, *J. Am. Helicopter Soc.*, 2022, **67**, pp 1–16. <https://doi.org/10.4050/JAHS.67.022011>
- [80] van der Wall, B.G., Lim, J.W., Smith, M.J., Jung, S., Bailly, J., Baeder, J. and Boyd, D.D. The HART II International Workshop: an assessment of the state of the art in comprehensive code prediction, *CEAS Aeronaut. J.*, 2013, **4**, (3), pp 223–252. <https://doi.org/10.1007/s13272-013-0077-9>
- [81] Smith, M.J., Lim, J.W., van der Wall, B.G., Baeder, J., Biedron, R.T., Boyd, D.D., Jayaraman, B., Jung, S. and Min, B.-Y. The HART II International Workshop: an assessment of the state-of-the-art in CFD/CSD prediction, *CEAS Aeronaut. J.*, 2013, **4**, (4), pp 345–372. <https://doi.org/10.1007/s13272-013-0078-8>
- [82] Smith, M.J., Jones, A., Ayancik, F., Mulleners, K. and Naughton, J. An assessment of the state of the art from the 2019 ARO dynamic stall workshop, AIAA-2020-2697, in *Aviation 2020 Forum*, June 2020. <https://doi.org/10.2514/6.2020-2697>
- [83] Smith, M.J., Gardner, A.D., Jain, R., Peters, D.A. and Richez, F. Rotating Wing dynamic stall: state of the art and future directions, in *Proceedings of the 76th Vertical Flight Society Annual Forum*, May/October 2020. <https://doi.org/10.4050/F-0076-2020-16472>
- [84] Smith, M.J. Computational vertical lift aeromechanics and its future in the 21st century, *J. Am. Helicopter Soc.*, 2025.
- [85] Goericke, J., Brenner, F. and Lee, D. Simulation and analysis of electric motor failure during eVTol aircraft operations in turbulent Airwake, in *50th European Rotorcraft Forum*, Marseille, France, Curran Associates, Red Hook, NY, September 10–12, 2024.
- [86] Smith, M.J., Bayoumi, A., Corman, J., et al. A Novel operational analysis tool for advanced air mobility, in *Proceedings of the VFS 81st Annual Forum*, Virginia Beach, VA, Curran Associates, May 20–22, 2025. <https://doi.org/10.4050/F-0081-2025-0259>
- [87] Branco, D.S., Stephens, I., White, M.D. and Watson, N.A. Assessing the interaction of helicopter rotor downwash and turbulent airwakes near hospital landing sites, in *50th European Rotorcraft Forum*, Marseille France, Curran Associates, Red Hook, NY, 2024.
- [88] Kurban, E., Oates, B., Smith, M.J. and Rauleder, J. Correlation of high and Mid Fidelity computational fluid dynamics for complex ship Airwake analysis, *AIAA J.*, 2025, In press. <https://doi.org/10.2514/1.C038087>
- [89] Jones, A.R., Cetiner, O. and Smith, M.J. Physics and modeling of large flow disturbances: discrete gust encounters for modern air vehicles, *Annu. Rev. Fluid Mech.*, 2022, **54**, pp 469–493. <https://doi.org/10.1146/annurev-fluid-031621-085520>
- [90] Salins, S., Crawford, A. and Smith, M.J. Estimation and tracking of maintenance and damage on advanced air mobility concepts,” in *Proceedings of the 50th European Rotorcraft Forum*, Marseille, France, Curran Associates, Red Hook, NY, September 10–12, 2024.
- [91] Bonnet, C., Kolpitke, A.G. and Smith, M. Computational validation and assessment of large amplitude transverse gust physics, *J. Am. Helicopter Soc.*, 2024, **69**, (2), p 020011. <https://doi.org/10.4050/JAHS.69.020011>
- [92] Corkery, S.J., Babinsky, H. and Graham, W.R. Quantification of added-mass effects using particle image velocimetry data for a translating and rotating flat plate, *J. Fluid Mech.*, 2019, **870**, pp 492–518. <https://doi.org/10.1017/jfm.2019.231>
- [93] Stutz, C., Hryniuk, J. and Bohl, D. Investigation of static wings interacting with vertical gusts of indefinite length at low Reynolds numbers, *Exp. Fluids*, 2022, **63**, (82). <https://doi.org/10.1007/s00348-022-03432-7>
- [94] Bonnet, C. Physics and Modeling of Nonlinear Sharp-Edged Transverse Gust Encounters and Applications to Urban Environments, PhD thesis, Georgia Institute of Technology, Atlanta, Georgia, 2024. <https://hdl.handle.net/1853/75616>.

- [95] Crawford, A. Fidelity assessments in computational prediction of unsteady loads for multi-rotor vehicles, PhD thesis, Georgia Institute of Technology, Atlanta, Georgia, 2025.
- [96] Wales, C., Jones, D. and Gaitonde, A. Prescribed velocity method for simulation of aerofoil gust responses, *J. Aircr.*, 2015, **52**, (1), pp 64–76. <https://doi.org/10.2514/1.C032597>
- [97] Corkery, S.J., Babinsky, H. and Harvey, J.K. On the development and early observations from a towing tank-based transverse Wing–Gust encounter test rig, *Exp. Fluids*, 2018, **59**, (9), p 135. <https://doi.org/10.1007/s00348-018-2586-0>
- [98] Ashok, S.G. and Rauleder, J. Real-time coupled ship–rotorcraft interactional simulations using GPU-accelerated Lattice-Boltzmann method, *J. Am. Helicopter Soc.*, 2025, **70**, p 022005. <https://doi.org/10.4050/JAHS.70.022005>
- [99] Ashok, S.G. and Rauleder, J. Mid-fidelity NATO generic destroyer static and moving-ship airwake simulations using the Lattice-Boltzmann method compared with experimental data, *Ocean Eng.*, 2024, **298**, p 117264. <https://doi.org/10.1016/j.oceaneng.2024.117264>
- [100] Waanders, D., Rauleder, J. and Smith, M.J. A real-time reduced-order model for the atmospheric boundary layer including roughness sublayer, in *Proceedings of the VFS 81st Annual Forum*, Curran Associates, May 20–22, 2025. <https://doi.org/10.4050/F-0081-2025-325>
- [101] Shenoy, R., Smith, M.J. and Park, M.A. Unstructured overset mesh adaptation with turbulence modeling for unsteady aerodynamic interactions, *J. Aircr.*, 2014, **51**, (1), pp 161–174. <https://doi.org/10.2514/1.C032195>
- [102] Lee, H., Save, A., Seshadri, P. and Rauleder, J. Large airfoil models, *arXiv e-prints*, 2024, pp arXiv:2410.08392. <https://doi.org/10.48550/arXiv.2410.08392>
- [103] Seth, D., Leishman, J.G., Gnanamanickam, E. and Zhang, Z. Time-resolved ship Airwake measurements in a simulated atmospheric boundary layer, *J Aircr.*, 2021, **58**, (3), pp 624–649. <https://doi.org/10.2514/1.C035886>
- [104] Zhu, N., Zhang, Z., Gnanamanickam, E. and Leishman, J.G. Space-time characterization of ship airwakes, *AIAA J.*, 2023, **61**, (2), pp 681–697. <https://doi.org/10.2514/1.J062093>
- [105] Oates, B., Vera Garcia, B., Rauleder, J. and Smith, M.J. Efforts toward a piecewise Reduced-Order model for unsteady, complex ship airwakes, in *Proceedings of the VFS 81st Annual Forum*, May 20–22, 2025. <https://doi.org/10.4050/F-0081-2025-0278>
- [106] Seeyave, J. and Smith, M.J. Spatio-temporal reduce order modelling of turbulent flow at very high Rernolds number using machine learning, in *Proposed for the 51st European Rotorcraft Forum, Marseille, France*, Curran Associates, Red Hook, NY, September 9–12, 2025.
- [107] Miki, K. and Menon, S. Local dynamic Subgrid closure for compressible MHD turbulence simulation,” in *37th AIAA Plasmadynamics and Lasers Conference*, June 5–8, 2006. <https://doi.org/10.2514/6.2006-2891>